iScience

CellPress
OPEN ACCESS

Article

Brain Hepcidin Suppresses Major Pathologies in Experimental Parkinsonism

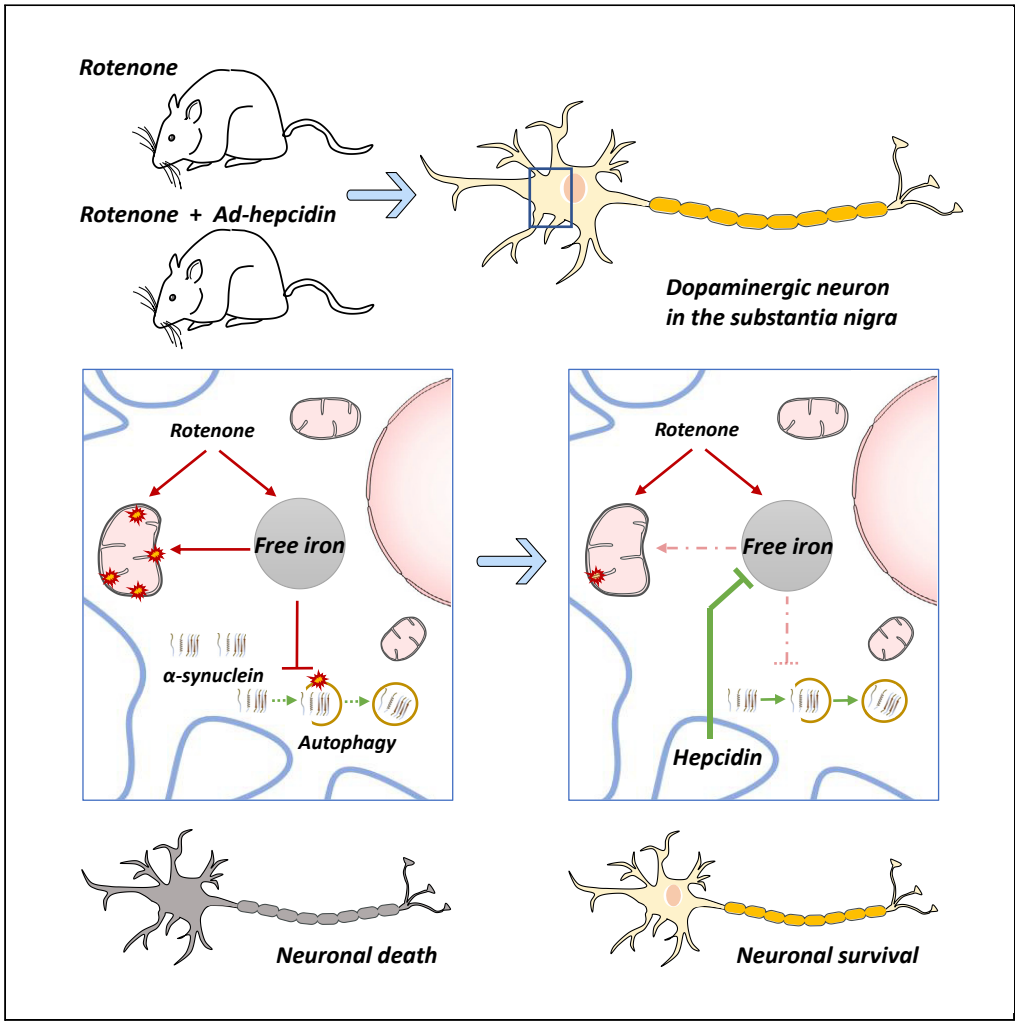

Tuo Liang, Zhong-Ming Qian, Ming-Dao Mu, Wing-Ho Yung, Ya Ke

yake@cuhk.edu.hk

HIGHLIGHTS

Hepcidin rescues motor deficits and dopaminergic neurodegeneration in PD models

Hepcidin represses iron accumulation and mitochondrial deficits in Parkinsonism

Hepcidin promotes clearance of α-synuclein via autophagy activation in PD model

Manipulating brain hepcidin level has potential application in treating PD

Liang et al., iScience *23*, 101284
July 24, 2020
https://doi.org/10.1016/j.isci.2020.101284

iScience

CellPress
OPEN ACCESS

Article

Brain Hepcidin Suppresses Major Pathologies in Experimental Parkinsonism

Tuo Liang,[1] Zhong-Ming Qian,[2] Ming-Dao Mu,[1,3] Wing-Ho Yung,[1,3] and Ya Ke[1,3,4,*]

SUMMARY

Despite intensive research on Parkinson disease (PD) for decades, this common neurodegenerative disease remains incurable. We hypothesize that abnormal iron accumulation is a common thread underlying the emergence of the hallmarks of PD, namely mitochondrial dysfunction and α-synuclein accumulation. We investigated the powerful action of the main iron regulator hepcidin in the brain. In both the rotenone and 6-hydroxydopamine models of PD, overexpression of hepcidin by means of a virus-based strategy prevented dopamine neuronal loss and suppressed major pathologies of Parkinsonism as well as motor deficits. Hepcidin protected rotenone-induced mitochondrial deficits by reducing cellular and mitochondrial iron accumulation. In addition, hepcidin decreased α-synuclein accumulation and promoted clearance of α-synuclein through decreasing iron content that leads to activation of autophagy. Our results not only pinpoint a critical role of iron-overload in the pathogenesis of PD but also demonstrate that targeting brain iron levels through hepcidin is a promising therapeutic direction.

INTRODUCTION

Parkinson disease (PD) is a progressive and incurable neurodegenerative disease, affecting 1%–2% of people older than 60 years (Hauser and Hastings, 2013). Patients suffering from PD exhibit characteristic motor dysfunctions, including rigidity, akinesia, tremor, and postural instability. The degeneration of dopaminergic neurons in the substantia nigra pars compacta (SNc) is the major cause of PD motor dysfunction. Currently, α-synuclein accumulation and mitochondrial dysfunction are two most common features and proposed causes of PD parthenogenesis (Haelterman et al., 2014; Grünewald et al., 2019; Charvin et al., 2018). α-Synuclein is the major component of Lewy bodies and neurites (Goedert, 2015). It is believed that aggregation of α-synuclein, which can severely impact proteasomes, lysosomes, mitochondria, endoplasmic reticulum (ER), and cell membrane aggregation, triggers the onset of PD (Dehay et al., 2016; Kalia et al., 2013). As for mitochondria dysfunction, findings from mitochondrial toxins, genetic studies, and patients suggest that it can be one of the general and primary causes of PD (Haelterman et al., 2014). In fact, α-synuclein accumulation and mitochondrial dysfunction might be linked during PD pathogenesis (Haelterman et al., 2014).

Iron accumulation is another pathological hallmark of PD. It has been reported by different groups that with disease progression, iron is gradually accumulated in the substantia nigra (SN) in PD patients (Ahmadi et al., 2020; Dexter et al., 1987; Ghassaban et al., 2019; Hirsch et al., 1991; Langley et al., 2019; Pyatigorskaya et al., 2015; Thomas et al., 2020). Consistent with this observation, in 6-hydroxydopamine (6-OHDA)- and 1-methyl-4-phenyl-1,2,3,6-tetrahydropyridine (MPTP)-induced PD animal models, iron levels are elevated in the SN concurrently with dopaminergic neuron loss, whereas iron chelator administration or iron-related gene rectification can ameliorate this impairment (Kaur et al., 2003; Shachar et al., 2004; Elkouzi et al., 2019; Crichton et al., 2019; Jiang et al., 2019; Nuñez and Chana-Cuevas, 2018). Iron accumulation and neurodegeneration are associated with altered expressions of iron-transport proteins, such as divalent metal transporter 1 (DMT1) with iron responsive element (DMT1+) (Jiang et al., 2010; Salazar et al., 2008; Urrutia et al., 2017a; Song et al., 2007; Chen et al., 2015). Increased free iron level causes neuronal damage and death not only via the Fenton reaction (Hadzhieva et al., 2014), which generates hydroxyl radicals that oxidize proteins, lipids, and DNA, but also affects the formation of α-synuclein oligomers in the presence of Fe^{3+} through a direct interaction (Levin et al., 2011). We speculate that iron accumulation, especially in free iron form, is a common thread connecting both mitochondrial dysfunction and α-synuclein aggregation in PD and that strategies that manipulate the level of iron would be highly beneficial. However, there is

[1]School of Biomedical Sciences, Faculty of Medicine, The Chinese University of Hong Kong, Shatin, Hong Kong, China

[2]Institute of Translational and Precision Medicine, Nantong University, Nantong 226001, China

[3]Gerald Choa Neuroscience Centre, The Chinese University of Hong Kong, Hong Kong, China

[4]Lead Contact

*Correspondence: yake@cuhk.edu.hk

https://doi.org/10.1016/j.isci.2020.101284

currently no applicable iron-modifying treatment for PD. Iron chelators have been investigated for clinical applications for several decades without success, although several new iron chelators seem to be promising in clinical trials recently (Devos et al., 2014; Moreau et al., 2018; Singh et al., 2019).

Hepcidin is a conserved 25-amino acid peptide that plays a key role in regulating iron metabolism (Hentze et al., 2010). Hepcidin is mainly produced in the liver to maintain iron homeostasis by regulating iron absorption in the intestine, iron recycling in the spleen, iron storage in the liver, and its utilization in the bone marrow (Hentze et al., 2010). Intriguingly, hepcidin is also expressed in the brain. Our previous work has demonstrated that hepcidin decreases iron uptake and release via decreasing the levels of DMT1+, DMT1 without IRE (DMT1−), transferrin receptor (TfR), and Fpn, in various types of cultured cells including astrocytes (Du et al., 2011), macrophages (Du et al., 2012), and microvascular endothelial cells (Du et al., 2015). In cultured neurons, hepcidin decreases DMT1, TfR, Fpn, ferritin-L, and ferritin-H contents (Zhou et al., 2017; Du et al., 2015). Recently, we found that hepcidin reduces brain iron in iron-overloaded rats and suppresses transport of transferrin-bound iron from the periphery into the brain (Du et al., 2015). Moreover, iron accumulation and oxidative stress are suppressed in the SN in iron-overloaded rats by hepcidin (Gong et al., 2016). However, whether hepcidin plays any role in central nervous system disease including PD is still to be investigated. Given its prominent iron-regulatory effect on brain iron accumulation, we hypothesize that hepcidin overexpression could be a promising strategy for treating PD.

In this study, we determined whether overexpression of hepcidin could rectify Parkinsonian symptoms and pathogenic changes in 6-OHDA- and rotenone-induced models of PD. We then investigated whether the beneficial effects of hepcidin are a result of amelioration of iron dyshomeostasis and other cellular dysfunctions in neurons. We found that hepcidin protects against rotenone-induced mitochondrial deficits by suppressing cellular and mitochondrial iron accumulation. In addition, it was revealed that hepcidin mediates α-synuclein clearance through decreasing iron accumulation and subsequent autophagy activation.

RESULTS

Therapeutic Effects of Hepcidin in PD Animal Models

We studied the potential therapeutic effects of hepcidin in two well-established rat models of PD, namely chronic IP administration of rotenone and acute unilateral 6-OHDA injections into the medial forebrain bundle. Although the neurotoxicology of these two models that lead to Parkinsonian symptoms are different (Blesa et al., 2012), iron accumulation is a shared feature (Mastroberardino et al., 2009). To assess the effect of hepcidin, we upregulated the expression of endogenous hepcidin in the brain by construction and injection of adenovirus that carries the hepcidin gene (Ad-hepcidin) (Du et al., 2015). In our previous study, we reported that after ICV injection of Ad-hepcidin, there were similar fold of increase of hepcidin mRNA levels in the cortex, hippocampus, and SN (Gong et al., 2016). The experimental paradigms of these sets of experiments are shown in Figures 1A and 1B. Overexpression of hepcidin in these two models by injection of Ad-hepcidin was confirmed by immunohistochemistry (Figures S1A and S1B) and ELISA (Figures S1C and S1D). Increased intensity of hepcidin was detected in neurons and glia in the SN (Figure S1A).

In the rotenone model, we tested the effects of Ad-hepcidin administration on motor ability of the rat using the catalepsy tests (grid test and bar test), stepping test, rotarod test, and ladder rung walking test 7 weeks after rotenone injection. Compared with the healthy control group, we found that rotenone treatment prolonged first-step latency in the grid test ($p < 0.01$) and latency to leave the bar in the bar test ($p < 0.05$). Injection of Ad-hepcidin but not the blank AAV (Ad-blank) reversed the prolonged latency in the grid test ($p < 0.05$, compared with rotenone group) and the bar test ($p < 0.05$, compared with rotenone group) (Figures 1C and 1D). In the stepping test, the numbers of adjusting steps of both the left and right paws were significantly reduced in rotenone-injected rats ($p < 0.01$, compared with the respective control). Similarly, Ad-hepcidin, but not Ad-blank, reversed the reduction in adjusting steps caused by rotenone ($p < 0.01$, compared with rotenone group) (Figures 1E and 1F). The beneficial effect of hepcidin overexpression in ameliorating Parkinsonian motor deficits was confirmed by the rotarod test and the ladder rung walking test (Figures S2A and S2B). Ad-hepcidin was also administered to normal rats without rotenone injection, and the motor ability of these rats did not differ from controls (Figures S3A and S3B). Consistent with these behavioral findings, immunohistochemical staining for tyrosine hydroxylase (TH) at the termination of experiments showed that rotenone caused severe reduction in TH immunoreactivity in the striatum (Figure S2C) and the number of TH-positive neurons in the SN (Figures 1G and 1H), which could be rescued by Ad-hepcidin, but not Ad-blank, treatment.

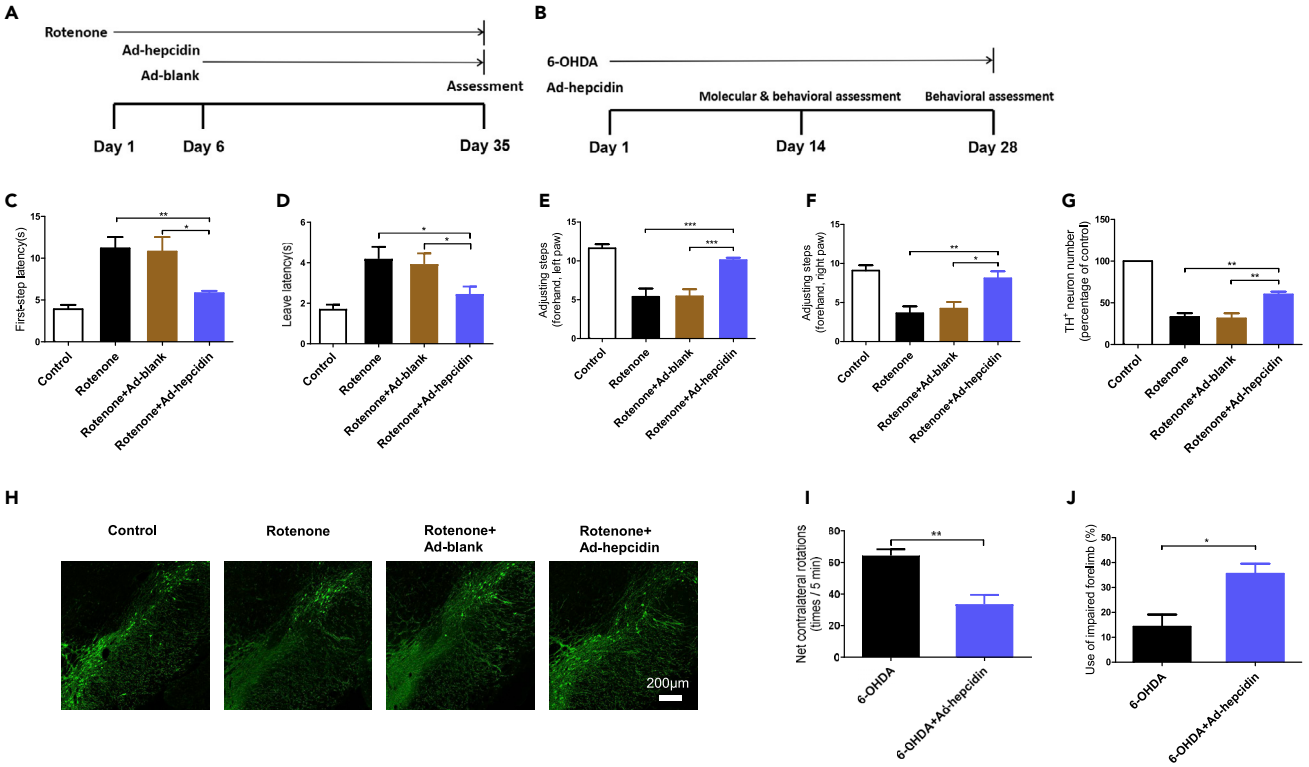

Figure 1. Ad-hepcidin Improved Rotenone-Induced Motor Deficiency and Dopaminergic Neuron Loss

Experimental scheme of rotenone and 6-OHDA model (A and B). Injection of rotenone (IP) induced a significant increase of first-step and descent latencies in grid and bar test, respectively, which was reduced by ICV Ad-hepcidin injection (C and D). In the stepping test, the reduction of adjusting steps induced by rotenone was also improved by Ad-hepcidin, for both the left and right paw (E and F). Tyrosine hydroxylase–positive (TH^+) neurons in the SNc were significantly reduced in count in rotenone treatment. Ad-hepcidin injection ameliorated TH^+ neuron loss. Quantitative analysis showed that the effect of Ad-hepcidin was statistically significant. Data were presented as percentage of control; the scale bar represents 200 μm (G and H). Ad-hepcidin injection into SN suppressed apomorphine-induced contralateral rotation in 6-OHDA model of PD (I). In the cylinder test, Ad-hepcidin ameliorated 6-OHDA-induced forelimb use asymmetry (J). *$p < 0.05$, **$p < 0.01$, ***$p < 0.001$, one-way ANOVA for C–G, two-tailed t test for I, J (n = 5–15 in each group); error bars, S.E.M.

In 6-OHDA-injected rats in which the motor function was affected unilaterally, we assessed the effects of hepcidin based on the forelimb cylinder test 2 weeks after 6-OHDA administration and the rotational behavior induced by R-(−)-apomorphine hydrochloride 4 weeks after 6-OHDA administration. Consistent with the rotenone model, upregulation of hepcidin rectified motor deficits in 6-OHDA-lesioned rats (Figures 1I and 1J). When compared with the unlesioned side, TH neurons were almost completely depleted in the SN of the lesioned side as revealed by TH-immunostaining ($p < 0.001$), whereas Ad-hepcidin rescued TH neurons significantly ($p < 0.01$) (Figures S2D and S2E).

Hepcidin Rectifies Iron Accumulation in Models of PD

To investigate the relationship between iron accumulation and hepcidin in the PD models, we determined the level of iron in the SN in rotenone- and 6-OHDA-treated rats and examined the effects of hepcidin. In rotenone-treated rats, neuronal loss was associated with deposition of iron within the SNc, where TH-positive dopaminergic neurons are located (Figure 2A). The morphology of the iron-stained spots is analogous to that of TH neurons, suggesting iron accumulation in the dopaminergic neurons in SNc. Concomitant with the effect in rescuing TH neuron loss, ICV injection of Ad-hepcidin, but not Ad-blank, suppressed iron accumulation in the SNc (Figure 2A). Consistently, the total iron level in the SN as measured by GFAAS was higher in rotenone-injected rats compared with control rats ($p < 0.05$), whereas Ad-hepcidin rather than Ad-blank rectified the abnormal iron levels ($p < 0.01$, compared with rotenone group, Figure 2B). Therefore, the protection conferred by hepcidin overexpression is likely related to reduced iron accumulation in the cell body of dopaminergic neurons in SNc.

As iron accumulation and neurodegeneration is associated with altered expressions of iron-transport proteins in several models of PD, we investigated whether the iron-suppressive effect of hepcidin is linked to

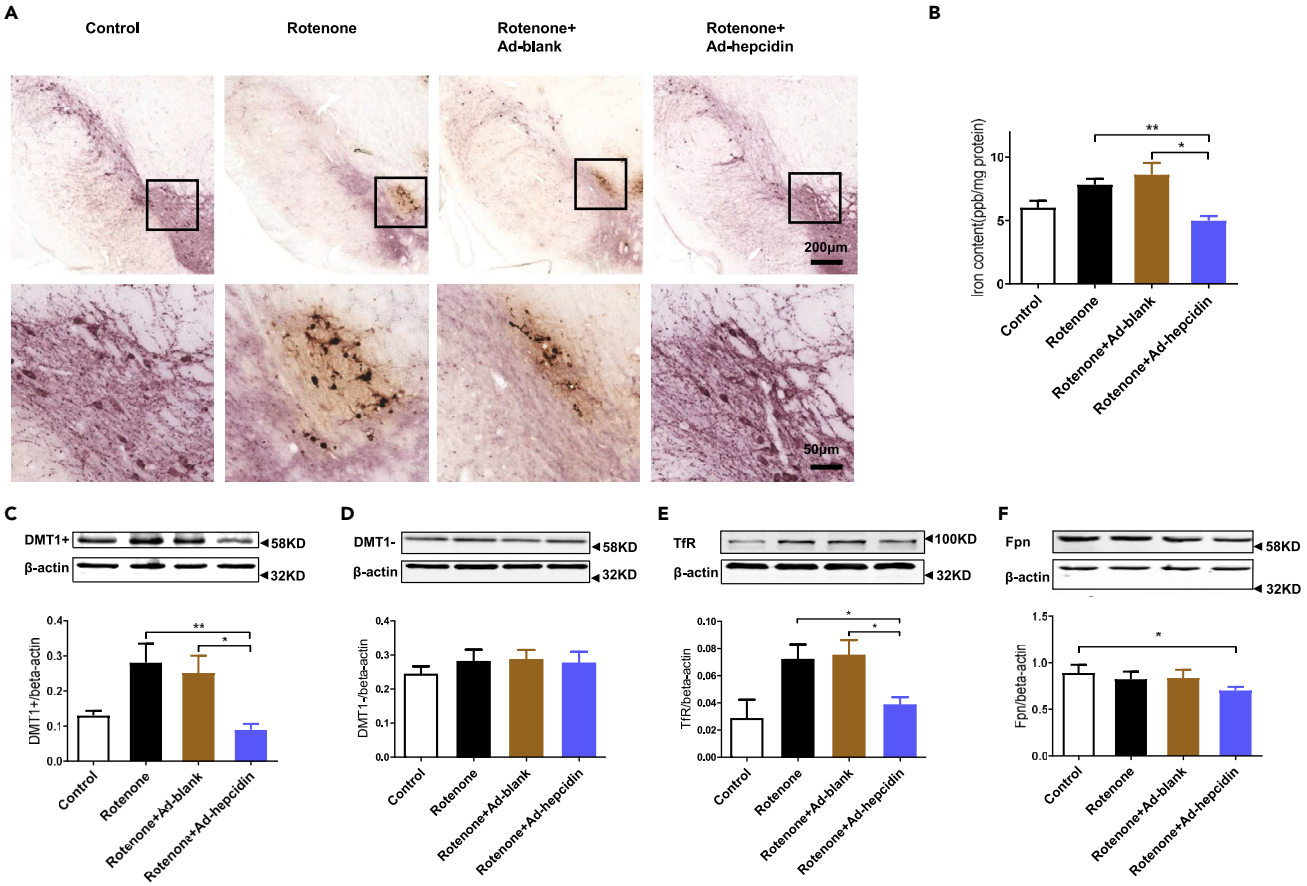

Figure 2. Ad-hepcidin Suppressed Rotenone-Induced Iron Accumulation in the SN via Regulating Iron-Transport Proteins

TH and iron co-staining revealed that rotenone treatment (IP) caused iron accumulation in the SNc. Ad-hepcidin injection (ICV) resulted in reduced accumulated iron in the SN. The scale bars represent 200 μm (top) and 50 μm (bellow) (A). Rotenone injection induced a significant iron content elevation in the SN, an effect that was blocked by Ad-hepcidin injection (B). DMT1+ and TfR were overexpressed in the SN in rotenone-injected rats. Ad-hepcidin suppressed rotenone-induced overexpression of DMT1+ and TfR (C and E). The levels of DMT1−were not affected by rotenone or Ad-hepcidin (D). Ad-hepcidin, but not rotenone, reduced the level of Fpn in the SN (F). *$p < 0.05$, **$p < 0.01$, one-way ANOVA (n = 5–10 for each group); error bars, S.E.M.

changes in the levels of iron-transport proteins in the SN. First, by western blot analysis, we found that rotenone-injected rats expressed much higher levels of DMT1+ in the SN ($p < 0.05$). Ad-hepcidin injection drastically decreased the DMT1+ levels ($p < 0.01$, compared with rotenone group, Figure 2C), but rotenone and Ad-hepcidin did not affect levels of DMT1− (Figure 2D). At the same time, the level of TfR was also higher in rotenone-injected rats ($p < 0.05$). Ad-hepcidin rather than Ad-blank downregulated TfR expression in rotenone-injected rats to a level that was comparable to that of the control ($p < 0.05$, Figure 2E). In addition, Ad-hepcidin, but not Ad-blank, led to a modest but significant decrease in the level of Fpn, the only iron export protein, in the SN ($p < 0.05$), although rotenone treatment did not affect Fpn level (Figure 2F). Thus, hepcidin could rectify the abnormal expressions of iron-import proteins associated with rotenone-induced Parkinsonism, with a slight suppression of iron export protein, contributing to iron suppression in SN. Ad-hepcidin was also administered to normal rats without rotenone injection, and DMT1+, TfR, and Fpn were found to be decreased compared with controls (Figures S3C–S3F).

Similarly, Ad-hepcidin effectively suppressed the iron deposition in the SN induced by 6-OHDA (Figure S4A). The iron repressive effect of hepcidin in 6-OHDA model was confirmed by measurement of iron content in the SN (Figure S4B). As for iron-transport proteins, 6-OHDA induced DMT1+ overexpression in the SN ($p < 0.01$), whereas Ad-hepcidin suppressed this effect ($p < 0.01$) (Figure S4C). Consistent with the rotenone model, 6-OHDA and hepcidin did not significantly affect DMT1− levels in the SN (Figure S4D). As for TfR, 6-OHDA induced its overexpression in the SN ($p < 0.05$), whereas Ad-hepcidin suppressed it ($p < 0.05$) (Figure S4E). Fpn was not significantly altered in the SN by 6-OHDA lesion, whereas

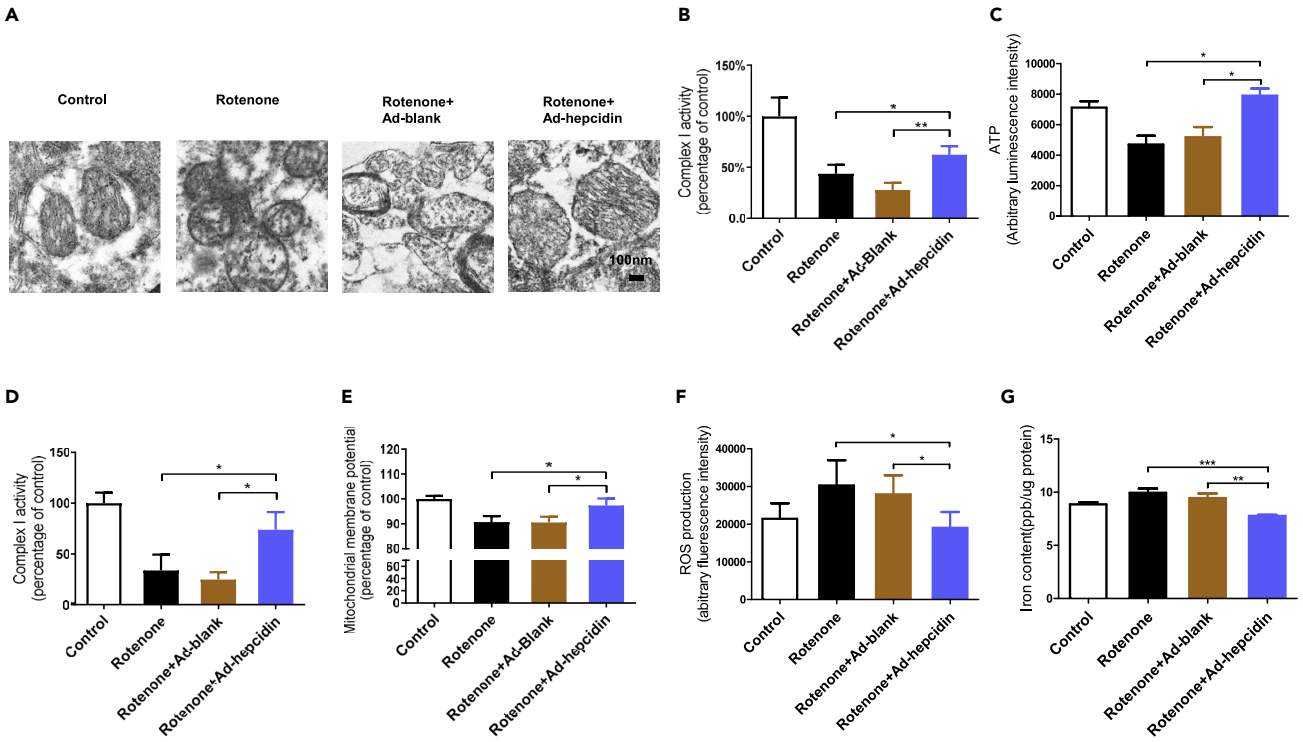

Figure 3. Ad-hepcidin Ameliorated Rotenone-Induced Mitochondrial Damage in the SN and the Whole Brain

Injection (IP) of rotenone caused severe mitochondrial malformation in the SN. The mitochondrial cristae were incomplete, whereas Ad-hepcidin injection (ICV) prevented the damage as revealed by transmission electron microscopy. The scale bar represents 100 nm (A). Ad-hepcidin rescued rotenone-induced mitochondrial complex I activity inhibition and ATP depletion in the SN. The data of Complex I activity were normalized to control, and the ATP levels were presented by arbitrary fluorescence intensity (B and C). Ad-hepcidin rescued rotenone-induced mitochondrial complex I activity inhibition, membrane potential decrease, and ROS overproduction in isolated mitochondria in rat brain. The data of complex I activity and membrane potential were normalized to controls (D–F). (G) Ad-hepcidin supressed rotenone-induced iron increase in isolated mitochondria in rat brain. *$p < 0.05$, **$p < 0.01$, one-way ANOVA (n = 5–10 in each group); error bars, S.E.M.

hepcidin downregulated its level ($p < 0.05$, Figure S4F). Therefore, hepcidin also rectifies the abnormal expression of iron transport proteins induced by 6-OHDA, which may account for its iron-suppressive effect in the SN.

We provided further evidence to suggest that the site of these changes were the dopaminergic neurons in the SNc. Thus, double staining of TH and iron transport proteins revealed overexpression of DMT1+ and TfR in the neuronal somata of TH-positive neurons in the SNc in rotenone-treated rats, which was suppressed by Ad-hepcidin but not Ad-blank (Figures S5A and S5B). On the other hand, in rotenone-treated rats, staining intensity of DMT1−was increased in the nucleus of TH^+ and other neurons, whereas Ad-hepcidin, but not Ad-blank, inhibited this change (Figure S5C). Also, Ad-hepcidin slightly decreased the fluorescence intensity of Fpn in the SN and TH^+ neurons (Figure S5D). All together, these results show that hepcidin specifically rectifies the anomalous expression of iron-transport proteins in dopaminergic neurons in the SN.

Hepcidin Ameliorates Mitochondrial Deficits in Rotenone-Induced Model of PD

Rotenone is well known to interfere with electron transport process in the mitochondria and mitochondrial function (Ahmed and Krishnamoorthy, 1992; Darrouzet et al., 1998; Gutman et al., 1970; Grivennikova et al., 1997; Ramsay and Singer, 1992). Hence, we examined the functional integrity of mitochondria in the PD models and the effects of hepcidin treatment. We first confirmed by electron microscopy that, under rotenone treatment, the mitochondria of neurons within the SNc appeared to be damaged in that the cristae were fragmented. Ad-hepcidin, but not Ad-blank, injection ameliorated such rotenone-induced mitochondrial malformation (Figure 3A). Moreover, in this model, rotenone induced inhibition of complex I activity ($p < 0.05$) and depleted ATP ($p < 0.05$) in the SN. These parameters were also restored by Ad-hepcidin but not Ad-blank ($p < 0.05$, compared with rotenone-treated group; Figures 3B and 3C).

To further pinpoint the site of action of hepcidin with respect to its protective function on the mitochondria, we isolated mitochondria directly from the brain and assessed different parameters. We found that in rotenone-treated animals, mitochondrial complex I activity was severely suppressed and the inner membrane potential significantly decreased ($p < 0.05$). On the other hand, ROS production was elevated ($p < 0.05$). These effects were largely rectified by Ad-hepcidin, but not Ad-blank, administration ($p < 0.05$, compared with rotenone group; Figures 3D–3F). Interestingly, in rotenone-treated rats, iron content in the isolated mitochondria was increased ($p < 0.05$), which was suppressed by Ad-hepcidin but not Ad-blank ($p < 0.001$, compared with rotenone group; Figure 3G), implicating a relationship between mitochondrial iron level and the protective effect of hepcidin on mitochondrial functions.

Hepcidin Rectifies Mitochondrial Deficits via Prevention of Iron Accumulation

We hypothesized that cellular and mitochondrial free iron accumulation is a prerequisite of severe mitochondria deficiency in PD, and the iron-repressive function of hepcidin accounts for its mitochondria protective effect. We studied the correlation between intracellular free ferrous iron level and mitochondrial activity by co-staining with Calcein-AM and TMRM in rotenone-treated SH-SY5Y cells. Calcein-AM intensity (green fluorescence) was negatively correlated to divalent ion level (mainly iron), whereas TMRM (red fluorescence) was positively correlated to mitochondrial membrane potential. In our experiments, rotenone treatment led to diminished Calcein-AM and TMRM fluorescence intensity, indicating iron accumulation and mitochondrial functional deficiency in SH-SY5Y cells, whereas co-treatment with hepcidin peptide (100nM) protected rotenone-treated cells from iron accumulation and mitochondrial damage. Importantly, co-treatment with $FeSO_4$ (5μM) blocked the effect of hepcidin on both decreasing iron level and protecting mitochondrial activity in these cells (Figure 4A). Thus, when the iron-suppressive effect of hepcidin was interfered by iron treatment, hepcidin had almost no effect on mitochondrial function.

In another set of experiments, we made use of RPA, a red fluorescent dye that can enter mitochondria, and the fluorescence intensity of which is negatively correlated with mitochondrial free iron level (Petrat et al., 2002; Rauen et al., 2003). We also made use of Rh-123, a green fluorescent dye that can enter mitochondria, and the fluorescent intensity of which is negatively correlated with mitochondrial membrane potential. In rotenone-treated cells, mitochondrial ferrous iron levels were raised, indicated by decreased red fluorescence intensity. Hepcidin peptide effectively prevented mitochondrial free iron accumulation, which was blocked by $FeSO_4$ (Figure 4B). Under this condition, hepcidin also failed to rescue rotenone-induced mitochondrial membrane potential decrease. These findings further support that hepcidin leads to mitochondrial iron decrease and protects mitochondria.

The above observations were verified by quantitative essays. In addition to signal changes of Calcein-AM (Figure 4C) and RPA intensity (Figure 4D) for semi-quantifying free ferrous iron level in the cells and mitochondria respectively, JC-1 was used as an indicator of mitochondrial membrane potential (Figure 4E). Our results confirmed that hepcidin is effective in protecting mitochondria by decreasing cellular and mitochondrial free iron accumulation.

Hepcidin Suppresses α-Synuclein Accumulation by Reducing Iron Accumulation

A distinct feature of the rotenone model of PD is the presence of α-synuclein accumulation in vulnerable areas of the brain, recapitulating a major pathological hallmark of human Parkinsonism. To test whether hepcidin can protect against α-synuclein accumulation in rotenone-induced rat model of PD, brain sections were co-stained for α-synuclein and TH. As shown in Figure 5A, in rotenone-treated rats, α-synuclein was expressed in the SNc. TH co-staining showed strong expression of α-synuclein in TH-positive neurons. When examining α-synuclein in higher magnification, we found clear discrete spots of immunofluorescence, suggesting aggregation of this protein within the TH neurons. Treatment with Ad-hepcidin, but not Ad-blank, suppressed rotenone-induced α-synuclein accumulation in TH^+ neurons.

Different forms of α-synuclein possess divergent solubility. Triton-soluble fraction represents normal α-synuclein. Some types of small α-synuclein oligomers are triton-insoluble SDS-soluble (Kostka et al., 2008), whereas many types of neurotoxic- and pathological-related α-synuclein dimers or oligomers are SDS-resistant (Levin et al., 2011; Kostka et al., 2008; Cappai et al., 2005; Grassi et al., 2018). The increased level of α-synuclein in SDS-resistant urea-soluble fraction also suggests aggregation of α-synuclein, which is a highly disease-associated event in PD patient and transgenic models (Lee et al., 2002; Kahle et al., 2001). Thereafter, proteins in the SN were isolated by Triton lysate, followed by SDS and urea. The levels

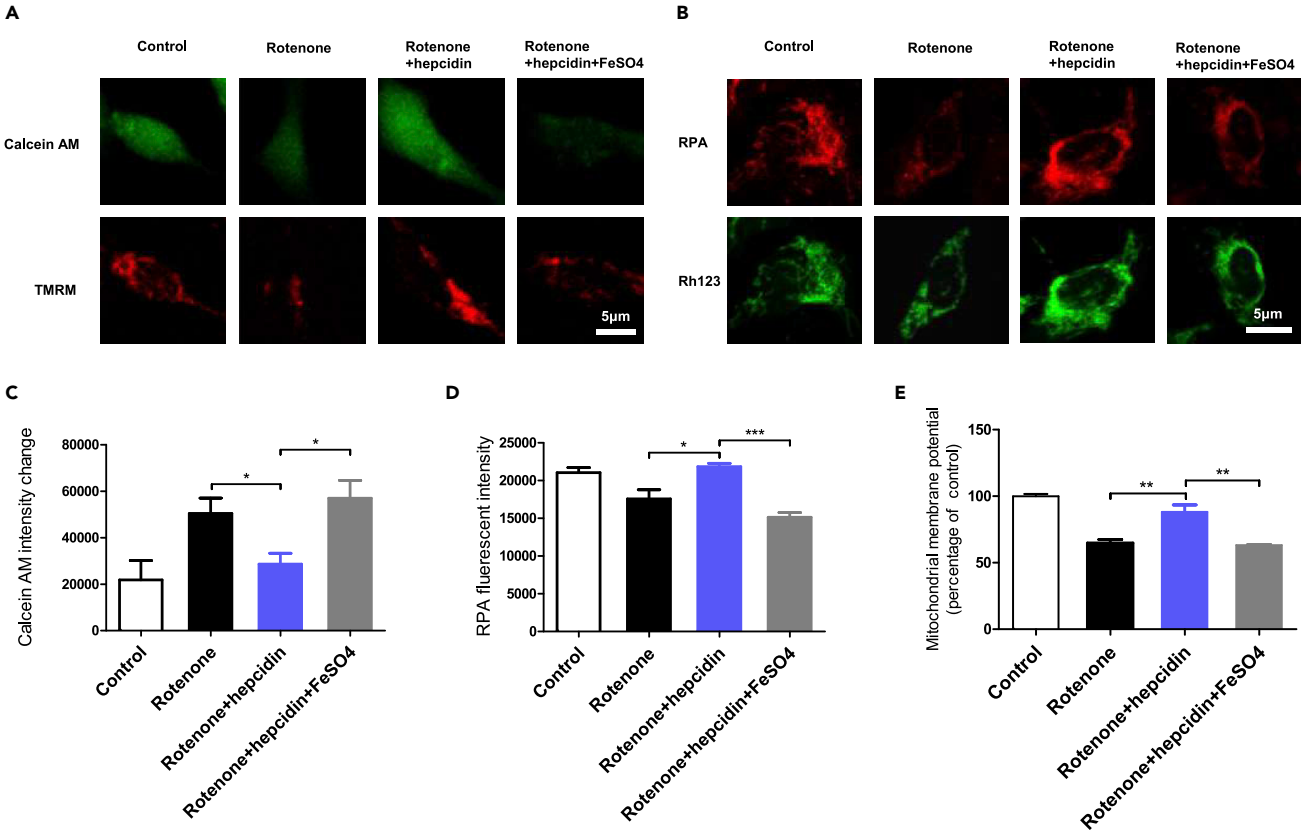

Figure 4. Hepcidin Ameliorated Rotenone-Induced Mitochondrial Damage via Suppressing Iron Accumulation

SH-SY5Y cells were treated with rotenone with or without hepcidin peptide for 24 h. Cells were co-stained with calcein-AM (green) and TMRM (red). Hepcidin reversed both rotenone-induced iron increase and mitochondrial membrane potential decrease, whereas $FeSO_4$ (5μM) treatment blocked the effect of hepcidin on cellular iron level and mitochondrial activity. The scale bar represents 5 μm (A). The SH-SY5Y cells were co-stained with RPA (red) and Rh123 (green). Rotenone treatment caused mitochondrial free ferrous iron accumulation, indicated by decreased RPA signal, whereas hepcidin suppressed these effects. $FeSO_4$ blocked the effect of hepcidin on mitochondrial iron level and activity in rotenone-treated cells. The scale bar represents 5 μm (B). The effect of iron treatment on intracellular ferrous iron levels was quantified using the calcein-AM method. $FeSO_4$ treatment blocked the effect of hepcidin on iron levels (C). The effect of iron treatment on mitochondrial free ferrous iron levels was measured using RPA. $FeSO_4$ treatment blocked the effect of hepcidin on mitochondrial iron levels (D). The cells were incubated with JC-1 dye, and the mitochondrial membrane potential was indicated by the ratio of red/green fluorescence intensity. Hepcidin suppressed rotenone-induced mitochondrial membrane potential decrease, whereas $FeSO_4$ blocked the effect of hepcidin on mitochondria. The data were normalized to control (E). *$p < 0.05$, **$p < 0.01$, one-way ANOVA ($n = 5–10$ in each group); error bars, S.E.M.

of α-synuclein were elevated in Triton ($p < 0.05$) and urea ($p < 0.05$) fractions but not SDS fractions in rotenone-treated rats. Ad-hepcidin abrogated rotenone-induced elevation of α-synuclein ($p < 0.05$, compared with rotenone group) (Figures 5B–5D). The above findings were also supported by *in vitro* studies in SH-SY5Y cells with some cells treated with rotenone (20nM) alone or rotenone (20nM) + hepcidin (100nM). Rotenone treatment caused dramatic α-synuclein accumulation in these cells, whereas hepcidin suppressed it (Figure 5E). Besides, the mRNA levels of α-synuclein was not altered either in the SN of rotenone-treated rats or in SH-SY5Y cells, and hepcidin did not affect mRNA levels of α-synuclein in both models (data not shown). Thus, both *in vitro* and *in vivo* evidence support that hepcidin inhibits α-synuclein accumulation in the rotenone model.

To establish a relationship between α-synuclein and iron accumulation under the effect of rotenone, we exploited the fact that α-synuclein accumulation can be induced in SH-SY5Y cells after prolonged rotenone treatment and that the iron-regulatory effect of hepcidin can be interfered by manipulation of iron content. Thus, in normal SH-SY5Y cells in which treatment with 20 nM of rotenone for more than 3 days caused α-synuclein accumulation ($p < 0.01$) (Figure 5F), a significant rise in cellular iron content was found in parallel ($p < 0.05$) (Figure 5G). Co-treatment with hepcidin suppressed the increases in both α-synuclein and iron content ($p < 0.05$). Consistent with the experiments on mitochondria, supplementation of exogenous $FeSO_4$

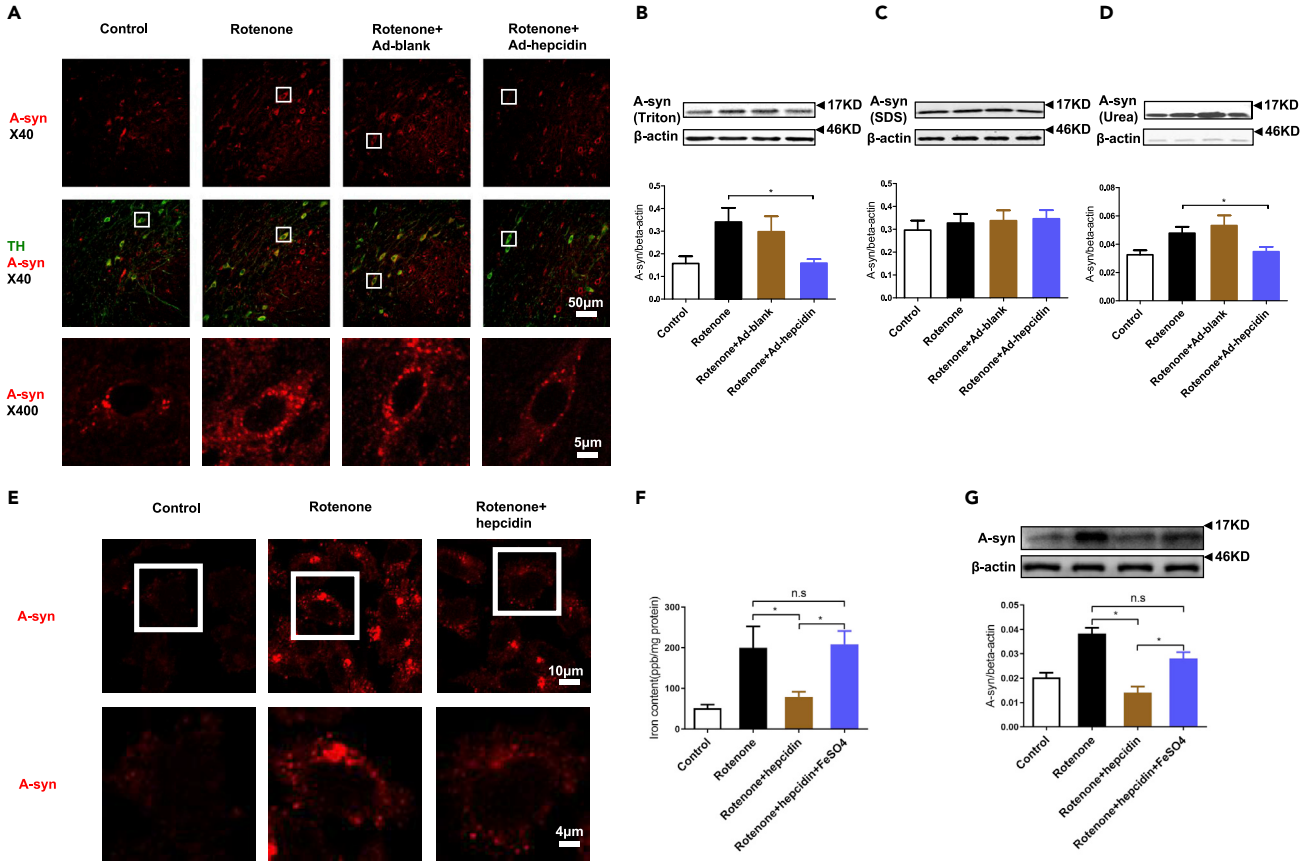

Figure 5. Hepcidin Decreased Rotenone-Induced α-Synuclein (A-syn) Accumulation via Decreasing Iron Content

Rotenone treatment (IP) caused A-syn accumulation in dopaminergic neurons in the SN, which was suppressed by Ad-hepcidin. The scale bars represent 50 μm (top) and 5 μm (bellow) (A). Proteins in the SN were fractionated by Triton, SDS, and urea. A-syn was increased in the Triton and urea fractions but not the SDS fraction, whereas Ad-hepcidin suppressed A-syn elevation in the Triton and urea fractions (B–D). Rotenone treatment caused A-syn accumulation in SH-SY5Y cells, whereas hepcidin peptide ameliorated it. The scale bars represent 10 μm (top) and 4 μm (bellow) (E). Levels of iron content were increased dramatically in rotenone-treated cells. Hepcidin treatment abrogated rotenone-induced iron increase in SH-SY5Y cells. $FeSO_4$ (5μM) treatment blocked hepcidin-medicated iron suppression (F). Hepcidin suppressed rotenone-induced A-syn accumulation in SH-SY5Y cells, an effect that was blocked by $FeSO_4$ treatment (G). *$p < 0.05$, n.s means no significant difference, one-way ANOVA (n = 5–10 in each group); error bars, S.E.M.

(5μM) eliminated the protective effects of hepcidin ($p < 0.05$) (Figures 5F and 5G). Together, these results strongly implicate that in the rotenone-induced model of PD, hepcidin inhibits α-synuclein accumulation via suppressing iron accumulation.

Hepcidin Mediates α-Synuclein Clearance via Iron Accumulation Suppression and Subsequent Activation of Autophagy

Because the accumulation, oligomerization, and aggregation of α-synuclein is generally regarded as toxic and could play a key role in the neurodegenerative process occurring in PD, elucidating how hepcidin can promote the clearance of this protein is an important question to address. It is known that some forms of SDS-resistant α-synuclein derives from incomplete autophagic degradation (Grassi et al., 2018), and the oligomerized and aggregated forms of α-synuclein are mainly degraded by the autophagy-lysosome system (Ebrahimi-Fakhari et al., 2011, 2012). Therefore, we asked whether rotenone and hepcidin exert any effect on the autophagy process. The levels of two autophagy markers, P62 and LC3B, were quantified in both the *in vivo* and *in vitro* rotenone models. In rotenone-treated rats, P62 was increased and the ratio of LC3B II/I was decreased in the SN ($p < 0.05$, Figures 6A and 6B), indicating suppression of autophagy. Ad-hepcidin, rather than Ad-blank, reduced P62 and raised the ratio of LC3BII/I, implying that hepcidin could induce autophagy ($p < 0.05$, compared with rotenone group, Figures 6A and 6B). Consistently, in SH-SY5Y cells, rotenone treatment induced an increase in P62 and a decrease in the ratio of LC3BII/I

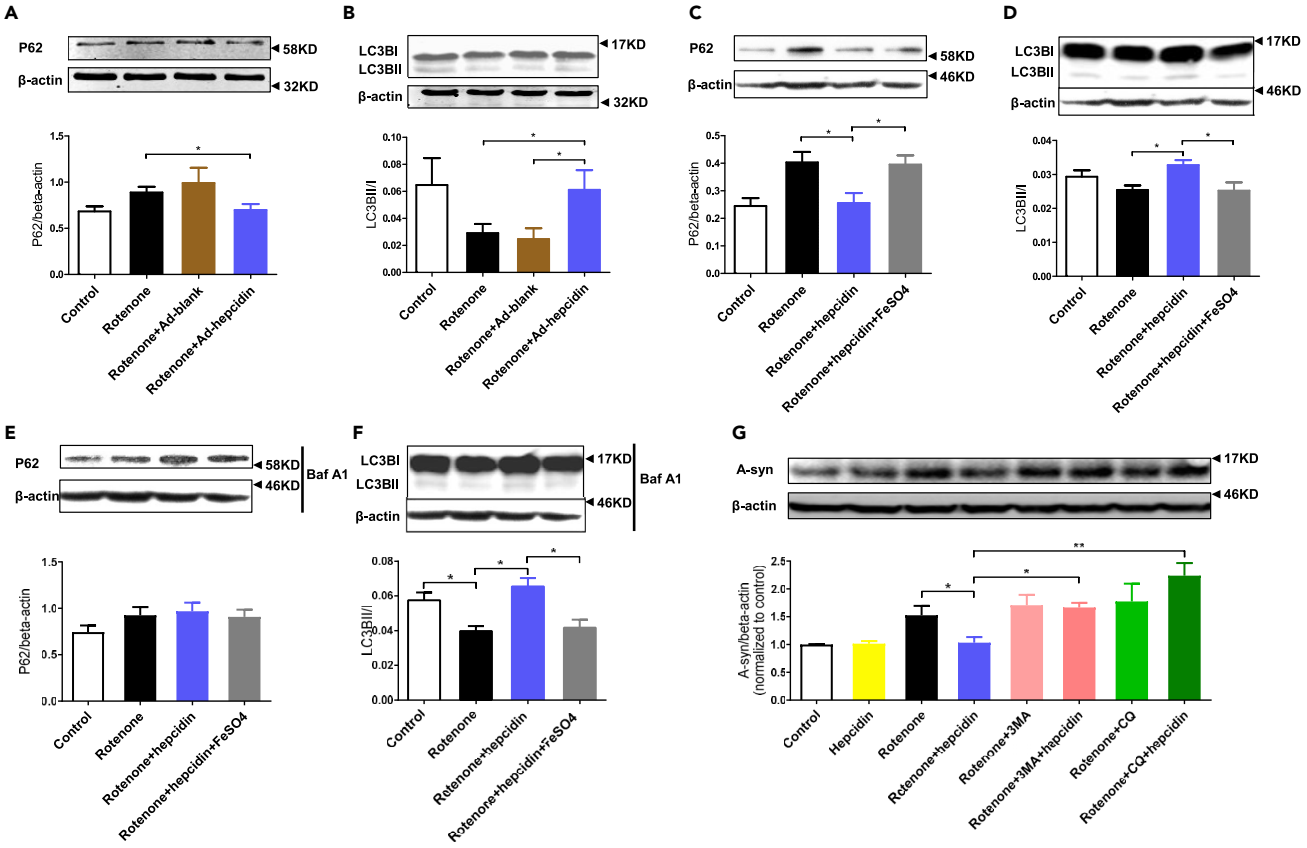

Figure 6. Hepcidin Mediated A-syn Clearance via Autophagy Activation

Rotenone treatment (IP) caused P62 accumulation and LC3BII/I ratio reduction in the SN, whereas Ad-hepcidin suppressed these effects (A and B). In SH-SY5Y cells, hepcidin suppressed rotenone-induced P62 accumulation and decrease of LC3BII/I ratio, an effect that was blocked by $FeSO_4$ (5μM) treatment (C and D). Baf A1 treatment caused P62 accumulation in all four groups, with a more significant rise of P62 in control and rotenone + hepcidin groups compared with the condition of no Baf A1 (C and E). Hepcidin failed to suppress P62 accumulation in rotenone-treated cells under Baf A1 treatment (E). Baf A1 treatment caused a general rise of LC3BII/I ratio in all of four groups (D and F). Hepcidin still increased the ratio of LC3BII/I when cells were treated with rotenone and Baf A1, an effect suppressed by $FeSO_4$ (F). Both autophagy inhibitor CQ and 3MA blocked hepcidin-mediated A-syn clearance in rotenone-treated SH-SY5Y cells. The data were normalized to control (G). *$p < 0.05$, **$p < 0.01$, one-way ANOVA (n = 5–10 in each group); error bars, S.E.M.

($p < 0.05$). These changes were reversed by hepcidin peptide (100nM) ($p < 0.05$ compared with rotenone group, Figures 6C and 6D). The cells were treated with bafilomycin A1 (Baf A1) (0.2 μM), an inhibitor of the late phase of autophagy, for 8 h before harvest, with increased P62 levels and LC3BII/I ratio in all groups observed. At the same time, Baf A1 failed to block rotenone-induced decrease of LC3BII/I ratio (Figures 6E and 6F), implying rotenone-induced autophagy initiation inhibition. In rotenone-treated cells, Baf A1 blocked hepcidin-mediated decrease of P62 but not the increase of LC3BII/I ratio ($p < 0.05$, compared with rotenone + hepcidin group), suggesting an activation of autophagy initiation by hepcidin (Figures 6E and 6F). In addition, the fact that addition of FeSO4 could abolish the effect of hepcidin on rotenone-induced changes in these markers ($p < 0.05$, compared with rotenone + hepcidin group) suggests the involvement of hepcidin-mediated reduction in iron level in the process (Figures 6C and 6D), that is, iron accumulation could be a cause of autophagy inhibition.

To elucidate whether hepcidin-mediated autophagy activation is responsible for α-synuclein clearance, we utilized a rotenone-induced *in vitro* model of PD. Both autophagy inhibitors, chloroquine (CQ) (10μM) and 3-Methyladenine (3MA) (5mM), blocked the effect of hepcidin in reversing rotenone-induced α-synuclein accumulation ($p < 0.05$, compared with rotenone + hepcidin group, Figure 6G). We also did parallel experiments on the proteasome system. As expected, hepcidin failed to ameliorate rotenone-induced inhibition of proteasome activity, and its mediation of α-synuclein clearance could not be blocked by proteasome inhibitor MG132 (2.5μM) in rotenone-treated cells (data not shown). Taken all together, we demonstrate

that hepcidin promotes α-synuclein clearance via specific autophagy activation in rotenone models, which is dependent on a reduction of free iron level.

DISCUSSION

In this study, we presented evidence supporting that iron accumulation could be a common thread of two major pathological hallmarks of PD, mitochondrial dysfunction and α-synuclein accumulation. More importantly, we found that suppression of iron accumulation in the brain by overexpression of hepcidin could rectify both mitochondrial dysfunction and α-synuclein accumulation in animal models of PD and achieve a therapeutic effect on motor deficits. The major experimental paradigm for the generation of Parkinsonism in this study is based on chronic administration of rotenone. Rotenone is known not only to cause highly selective nigrostriatal dopaminergic degeneration and motor deficits, including bradykinesia, postural instability, and rigidity, but also to result in fibrillar cytoplasmic inclusions that contain α-synuclein and ubiquitin in dopaminergic neurons of the SN (Betarbet et al., 2000, 2006; Feng et al., 2006; Cannon et al., 2009). Furthermore, chronic rotenone treatment on differentiated SH-SY5Y cells reproduces Lewy neurites with accumulated α-synuclein (Borland et al., 2008).

Although mounting evidence suggests that iron is accumulated in the SN together with mitochondrial deficits in PD, the mechanistic link, if any, between these two phenomena has not been established firmly. It has been proposed that proteins containing Fe-S clusters in mitochondria and IRP1 could be the causal link between mitochondrial damage and consequential mitochondrial and cytoplasmic iron increase (Muñoz et al., 2016; Liddell and White, 2018; Cerri et al., 2019; Mena et al., 2011, 2015b). Meanwhile, it had been reported that mitochondrial health and iron homeostasis are co-regulated by Nrf2, a redox-sensitive transcription factor (Ammal Kaidery et al., 2019). However, whether mitochondrial and cytoplasmic labile iron increase is a prerequisite for mitochondria deficits and effective treatment targeting excess iron to rescue mitochondria have not been well explored. In a previous *in vitro* study on midbrain dopaminergic neurons, MPTP induced overexpression of DMT1 and iron influx together with a mitochondria membrane potential decrease, whereas DFO, the iron chelator, abolished all of these effects (Zhang et al., 2009). As DFO is unable to pass through the mitochondrial membrane and chelate mitochondrial iron, the protective effect of DFO implies that iron outside the mitochondria exacerbates mitochondrial damage. However, a group recently reported that chelators that mainly decrease mitochondrial iron pool was much more effective than those that decrease the cytoplasmic iron pool, indicating that the mitochondrial iron pool plays a more important role in mitochondrial intoxication (Mena et al., 2015a). These studies implicate that excessive free iron accumulation could account for mitochondria deficiency in PD. Our result that hepcidin ameliorated rotenone-induced mitochondrial malformation and deficiency in the SN supports this notion. Thus, natural iron-regulatory protein can be as effective as iron chelators in regulating mitochondrial iron dyshomeostasis. These findings are in line with previous studies showing that mitochondrial ferritin, an iron storage protein specifically located in mitochondria that possesses high homology to H-ferritin (Levi et al., 2001), could protect mitochondria and suppress ROS and dopaminergic neural loss in both 6-OHDA- and MPTP-induced PD models (Shi et al., 2010; You et al., 2016).

Our finding on the effects of hepcidin in α-synucleinopathy is of particular interest. Phosphorylated α-synuclein fibrils are the major constituent of Lewy neurites and Lewy bodies, which are the hallmarks of PD. Most α-synuclein in SDS-insoluble urea-soluble fraction is phosphorylated at Ser129, whereas normal α-synuclein in Triton fraction is not (Fujiwara et al., 2002). Except fibrils, phosphorylated α-synuclein dimer that induces mitochondrial deficits is also SDS resistant (Grassi et al., 2018). Besides, α-synuclein forms various SDS-resistant oligomers that are toxic to cells, such as species induced by Fe^{3+} or dopamine (Kostka et al., 2008; Cappai et al., 2005). In the present study, SDS-resistant α-synuclein was elevated in rotenone-treated rats, whereas hepcidin exerted strong suppressive effect, suggesting repression of PD pathogenesis. The interaction between iron accumulation and α-synucleinopathy in PD has also been documented. Iron accumulation occurs in the SN where Lewy bodies are also abundantly present (Li et al., 2010; Spillantini et al., 1997), and ferrous and ferric iron are observed to be present in Lewy bodies (Peng et al., 2010). In *ex vivo* experiments, iron directly interacts with α-synuclein and promotes its oligomerization and fibrillization (Joppe et al., 2019). Several *in vitro* experiments also imply post-transcriptional regulation of α-synuclein by iron via IRP-IRE signaling pathway (Chen et al., 2019). As for α-synuclein degradation, iron may suppress the proteasomal degradation of α-synuclein by inactivating Parkin (Ganguly et al., 2020). In this study, we confirmed that iron accumulation is one of the major causes of α-synucleinopathy and found that hepcidin suppressed autophagic flux inhibition via decreasing overloaded free

iron, thereby promoting autophagic degradation of α-synuclein. The autophagy-lysosomal pathway is the major pathway for α-synuclein degradation during increased α-synuclein burden or when α-synuclein is aggregated. However, this pathway may be impaired in PD. In sporadic PD patients, the activity of α-galactosidase A, a lysosomal hydrolase, is significantly decreased (Wu et al., 2011). Moreover, it has been widely reported that boosting autophagy promotes α-synuclein clearance and protects neurons in PD models (Dehay et al., 2010; Lonskaya et al., 2013; Jang et al., 2016; Hou et al., 2015). In addition, iron chelator DFO induced autophagy and exerted its protective effects in rotenone-treated SH-SY5Y cells (Wu et al., 2010). Taken all together, our results suggest that iron accumulation plays role in autophagy flux inhibition and subsequent α-synuclein accumulation in PD, whereas rectifying iron homeostasis via hepcidin can reduce free iron, activate autophagy, and promote α-synuclein clearance.

The iron-suppressing effect of hepcidin in dopaminergic neurons is predominantly achieved through the suppression of DMT1+ and TfR, the two major iron import proteins, responsible for non-transferrin bound iron and transferrin bound iron import, respectively. In fact, both DMT1+ and TfR have consistently been implicated in human PD as well as animal models of PD (Jiang et al., 2010; Aguirre et al., 2012; Jia et al., 2015; Salazar et al., 2008). The inhibitory effect of hepcidin on iron uptake in neurons have been reported by us previously (Zhou et al., 2017; Du et al., 2015), and the mechanism may be the same as in astrocytes and macrophages, which is via cAMP-PKA pathway (Du et al., 2011, 2012). Fpn is the only identified iron export protein as well as the target of hepcidin located on the cell membrane. However, hepcidin-mediated Fpn reduction in dopaminergic neurons does not appear to contribute to the effect. Despite some studies revealing coincidence of changed Fpn levels in the SN and the fate of dopaminergic neurons (Xu et al., 2017; Lee et al., 2009; Finkelstein et al., 2017; Lv et al., 2011; Zhang et al., 2014) in PD models and the detrimental effect of Fpn silencing in 6-OHDA-treated cultured cells (Song et al., 2010), there are other studies showing that Fpn deletion has no apparent consequence on dopaminergic neurons in the SN in mice (Matak et al., 2016). Ferrous iron is exported by Fpn following oxidation by ceruloplasmin (CP), a protein that has been shown to be associated with PD (Wang and Wang, 2019). However, the link between CP and Fpn in dopaminergic degeneration is not clear and worth to be investigated in the future. Secondly, hepcidin still suppresses iron uptake in iron-depleted cells, indicating that the inhibitory effect of hepcidin on iron uptake is not a feedback of hepcidin-mediated Fpn degradation and subsequent iron increase (Du et al., 2011). Thirdly, cyclic adenosine monophosphate is normally a second messenger response to hormone receptors located on the membrane of target cell (Qian and Ke, 2019), which implies the existence of an unidentified receptor of hepcidin. Except repressing iron uptake in dopaminergic neurons, given that hepcidin reduces iron transport across the blood-brain barrier (BBB) in normal and iron overload conditions via regulating DMT1 and TfR (Du et al., 2015; McCarthy and Kosman, 2014), as proposed in a ''bypass model''(Du et al., 2015; Qian and Ke, 2019), and the properties of the BBB are altered in PD (Stolp and Dziegielewska, 2009), it is probable that hepcidin ameliorates rotenone-induced neuronal degeneration and iron accumulation partially via suppressing iron import into brain. In summary, although Ad-hepcidin also decreased Fpn expression, we found that suppression of iron influx is the overwhelming effect of hepcidin in the SN. Nevertheless, to establish a clear causal relation between hepcidin-mediated iron reduction and other beneficial effects of hepcidin, identifying the receptor of hepcidin or manipulation of hepcidin-regulated iron proteins is warranted in future studies.

As an endogenous cationic hormone containing 25 amino acids, it has been reported that hepcidin can cross the BBB (Raha-Chowdhury et al., 2015; Xiong et al., 2016; Vela, 2018), although the permeability is not yet determined. To increase the penetration rate across the BBB, hepcidin can be conjugated with plasma membrane transducing domains (Murriel and Dowdy, 2006), or ligands targeting receptors on the BBB, notably transferrin or TfR monoclonal antibodies (Angeli et al., 2019; Pardridge, 2015). Alternative approaches that are potentially feasible include delivery by nanoparticles (Grabrucker et al., 2016; Angeli et al., 2019) and the use of hepcidin agonists (Casu et al., 2018).

It is noteworthy that hepcidin has a dual role in diseases associated with inflammation and iron overload (Vela, 2018). Hepcidin is an antimicrobial peptide that is overproduced under infection, inflammation, and stress as an innate defense mechanism. A consensus on whether hepcidin overexpression in different disease models is beneficial or detrimental has not been reached. For example, hepcidin could exacerbate brain damage in ischemic or hemorrhagic stroke (Tan et al., 2016; Ding et al., 2011; Xiong et al., 2016), whereas it has been reported to be protective in iron overload condition and Alzheimer disease (AD) (Gong et al., 2016; Urrutia et al., 2017b). One possibility is that the timing of hepcidin is critical, being

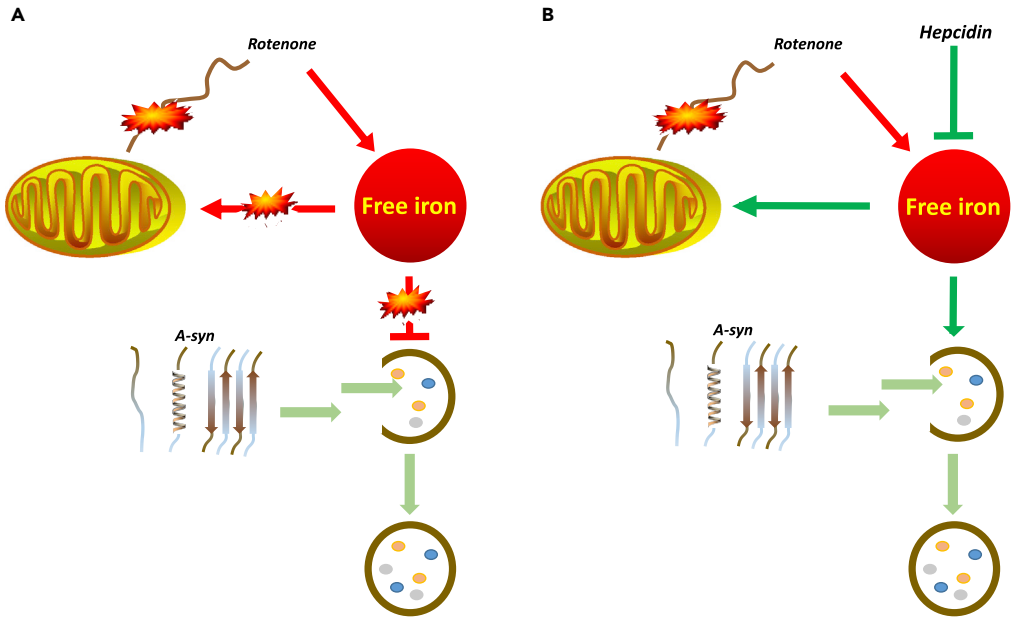

Figure 7. A Model of Mechanism of Action of Hepcidin

Rotenone treatment causes mitochondrial damage and iron accumulation in dopaminergic neurons in the substantia nigra. Iron accumulation exacerbates mitochondrial damage. At the same time, overloaded iron results in autophagy inhibition leading to alpha-synuclein (A-syn) accumulation (A). The major action of hepcidin is the abrogation of rotenone-induced iron increase. Consequently, mitochondrial damage is ameliorated, and A-syn is degraded by the activation of autophagy (B).

beneficial mainly in pre-treatment (Vela, 2018). However, given that we did not pre-treat hepcidin in our model, differences in the nature of disease may account for the observed differences. Specifically, stroke is a disease with acute and severe damage to BBB and neurons, whereas in neurodegenerative diseases neurons are damaged chronically usually with years of progression. Inflammation is far more severe in stroke than in neurodegenerative diseases (Wang et al., 2018; Mracsko and Veltkamp, 2014; Stephenson et al., 2018), with notable differences in roles of immunocytes between ischemic stroke and neurodegenerative diseases (Rosset et al., 2015; Zhu et al., 2019; Solleiro-Villavicencio and Rivasarancibia, 2018; Gonzalez and Pacheco, 2014; Brochard et al., 2008; Kustrimovic et al., 2019; Chen et al., 2018). Given that AD and PD share some common mechanisms of iron metabolism and hepcidin is also decreased in the brain in AD animal models and patients (Raha et al., 2013), it is reasonable to speculate a similar protective role of hepcidin in PD. Also, it is possible that microglia, astrocytes, and the peripheral immune system all contribute to neurotoxin-induced dopaminergic neuronal degeneration. Inflammation could be triggered by mitochondrial damage and α-synucleinopathy (Geto et al., 2020; Gelders et al., 2018; Troncosoescudero et al., 2018) and acts as an amplifier of degenerative events including aggravating mitochondrial damage and iron accumulation in neurons via cytokines, ROS, and TLRs signal in PD (Urrutia et al., 2014; Trudler et al., 2015). Nonetheless, our *in vitro* experiments demonstrated effectiveness of hepcidin on cultured neurons. Meanwhile, 6-OHDA and rotenone not only primarily and selectively damage dopaminergic neurons *in vivo* but also cause neurodegeneration and iron accumulation without glia in *in vitro* studies (Mouhape et al., 2019; Workman et al., 2015; Mena et al., 2011; Jia et al., 2015). Moreover, a direct pathway from mitochondria dysfunction to Fe-S proteins-mediated iron accumulation in neurons without involvement of inflammation in early steps has been reported (Urrutia et al., 2014; Muñoz et al., 2016; Mena et al., 2015b). Thus, a direct action on dopaminergic neurons rather than glia is believed to be a more important protective mechanism of hepcidin in the present study.

In conclusion, our study demonstrates the beneficial effect of hepcidin in PD animal models and elucidates the mechanism in neurons, which is summarized in Figure 7. On a broader perspective, our study confirms the detrimental effect of iron overload in the pathogenic process of Parkinsonism. Rectifying iron dyshomeostasis via manipulation of hepcidin level in the brain could suppress iron accumulation and other major pathologies of PD and therefore represents a promising therapeutic direction.

Limitations of the Study

As discussed earlier, the limitation of present study is that whether the beneficial effect of hepcidin on dopaminergic neurons is also via modulation of inflammation in PD. Besides, the contribution of glia cells in the protective process is not experimentally addressed.

Resource Availability

Lead Contact

Further information and requests for resources and reagents should be directed to and will be fulfilled by the Lead Contact, Ya Ke (yake@cuhk.edu.hk).

Materials Availability

Viruses generated in this study will be made available on request, but we may require a payment and/or a completed Materials Transfer Agreement if there is potential for commercial application.

Data and Code Availability

Raw data will be shared upon receipt of a reasonable request.

METHODS

All methods can be found in the accompanying Transparent Methods supplemental file.

SUPPLEMENTAL INFORMATION

Supplemental Information can be found online at https://doi.org/10.1016/j.isci.2020.101284.

ACKNOWLEDGMENTS

This work was supported by the Hong Kong Research Grants Council (HKRGC)-General Research Fund,14107616,14167817 (Y.K.), Hong Kong Research Grants Council, Hong Kong, China, HKRGC-Collaborative Research Fund C6004-17G (W.H.Y.), Health and Medical Research Fund, Hong Kong, 01120146, and a National Natural Science Foundation of China grant NSFC31571195 (Z.M.Q.)

AUTHOR CONTRIBUTIONS

Y.K. conceived the project, designed the experiments, analyzed the data, and supervised the project. W.H.Y. and Z.M.Q. designed the experiments, supervised the studies, and analyzed the data. T. L and M.D.M. performed the experiments, analyzed the data, and prepared the figures. Y.K. wrote the manuscript. All authors read and approved the final manuscript.

DECLARATION OF INTERESTS

The authors declare no competing interests.

Received: February 20, 2020
Revised: April 26, 2020
Accepted: June 15, 2020
Published: July 24, 2020

REFERENCES

Aguirre, P., Urrutia, P., Tapia, V., Villa, M., Paris, I., Segura-Aguilar, J., and Nunez, M.T. (2012). The dopamine metabolite aminochrome inhibits mitochondrial complex I and modifies the expression of iron transporters DMT1 and FPN1. Biometals *25*, 795–803.

Ahmadi, S.A., Bötzel, K., Levin, J., Maiostre, J., Klein, T., Wein, W., Rozanski, V., Dietrich, O., Ertl-Wagner, B., Navab, N., and Plate, A. (2020). Analyzing the co-localization of substantia nigra hyper-echogenicities and iron accumulation in Parkinson's disease: a multi-modal atlas study with transcranial ultrasound and MRI. Neuroimage Clin. *26*, 102185.

Ahmed, I., and Krishnamoorthy, G. (1992). The non-equivalence of binding sites of coenzyme quinone and rotenone in mitochondrial NADH-CoQ reductase. FEBS Lett. *300*, 275–278.

Ammal Kaidery, N., Ahuja, M., and Thomas, B. (2019). Crosstalk between Nrf2 signaling and mitochondrial function in Parkinson's disease. Mol. Cell. Neurosci. *101*, 103413.

Angeli, E., Nguyen, T.T., Janin, A., and Bousquet, G. (2019). How to make anticancer drugs cross the blood-brain barrier to treat brain metastases. Int. J. Mol. Sci. *21*, 22.

Betarbet, R., Canet-Aviles, R.M., Sherer, T.B., Mastroberardino, P.G., McLendon, C., Kim, J.H., Lund, S., Na, H.M., Taylor, G., Bence, N.F., et al. (2006). Intersecting pathways to neurodegeneration in Parkinson's disease: effects of the pesticide rotenone on DJ-1, alpha-synuclein, and the ubiquitin-proteasome system. Neurobiol. Dis. *22*, 404–420.

Betarbet, R., Sherer, T.B., Mackenzie, G., Garcia-Osuna, M., Panov, A.V., and Greenamyre, J.T. (2000). Chronic systemic pesticide exposure reproduces features of Parkinson's disease. Nat. Neurosci. *3*, 1301–1306.

Blesa, J., Phani, S., Jackson-Lewis, V., and Przedborski, S. (2012). Classic and new animal models of Parkinson's disease. J. Biomed. Biotechnol. *2012*, 845618.

Borland, M.K., Trimmer, P.A., Rubinstein, J.D., Keeney, P.M., Mohanakumar, K., Liu, L., and Bennett, J.P., Jr. (2008). Chronic, low-dose rotenone reproduces Lewy neurites found in early stages of Parkinson's disease, reduces mitochondrial movement and slowly kills differentiated SH-SY5Y neural cells. Mol. Neurodegener *3*, 21.

Brochard, V., Combadiere, B., Prigent, A., Laouar, Y., Perrin, A., Berayberthat, V., Bonduelle, O., Alvarezfischer, D., Callebert, J., and Launay, J. (2008). Infiltration of CD4+ lymphocytes into the brain contributes to neurodegeneration in a mouse model of Parkinson disease. J. Clin. Invest. *119*, 182–192.

Cannon, J.R., Tapias, V., Na, H.M., Honick, A.S., Drolet, R.E., and Greenamyre, J.T. (2009). A highly reproducible rotenone model of Parkinson's disease. Neurobiol. Dis. *34*, 279–290.

Cappai, R., Leck, S.L., Tew, D.J., Williamson, N.A., Smith, D.P., Galatis, D., Sharples, R.A., Curtain, C.C., Ali, F.E., Cherny, R.A., et al. (2005). Dopamine promotes alpha-synuclein aggregation into SDS-resistant soluble oligomers via a distinct folding pathway. FASEB J. *19*, 1377–1379.

Casu, C., Nemeth, E., and Rivella, S. (2018). Hepcidin agonists as therapeutic tools. Blood *131*, 1790–1794.

Cerri, S., Milanese, C., and Mastroberardino, P.G. (2019). Endocytic iron trafficking and mitochondria in Parkinson's disease. Int. J. Biochem. Cell Biol. *110*, 70–74.

Charvin, D., Medori, R., Hauser, R.A., and Rascol, O. (2018). Therapeutic strategies for Parkinson disease: beyond dopaminergic drugs. Nat. Rev. Drug Discov. *17*, 844.

Chen, B., Wen, X., Jiang, H., Wang, J., Song, N., and Xie, J. (2019). Interactions between iron and α-synuclein pathology in Parkinson's disease. Free Radic. Biol. Med. *141*, 253–260.

Chen, D., Kanthasamy, A.G., and Reddy, M.B. (2015). EGCG protects against 6-OHDA-induced neurotoxicity in a cell culture model. Parkinsons Dis. *2015*, 843906.

Chen, Z., Chen, S., and Liu, J. (2018). The role of T cells in the pathogenesis of Parkinson's disease. Prog. Neurobiol. *169*, 1–23.

Crichton, R.R., Ward, R.J., and Hider, R.C. (2019). The efficacy of iron chelators for removing iron from specific brain regions and the pituitary-ironing out the brain. Pharmaceuticals (Basel) *12*, 138.

Darrouzet, E., Issartel, J.P., Lunardi, J., and Dupuis, A. (1998). The 49-kDa subunit of NADH-ubiquinone oxidoreductase (Complex I) is involved in the binding of piericidin and rotenone, two quinone-related inhibitors. FEBS Lett. *431*, 34–38.

Dehay, B., Bove, J., Rodriguez-Muela, N., Perier, C., Recasens, A., Boya, P., and Vila, M. (2010). Pathogenic lysosomal depletion in Parkinson's disease. J. Neurosci. *30*, 12535–12544.

Dehay, B., Decressac, M., Bourdenx, M., Guadagnino, I., Fernagut, P.O., Tamburrino, A., Bassil, F., Meissner, W.G., and Bezard, E. (2016). Targeting α-synuclein: therapeutic options. Mov. Disord. *31*, 882–888.

Devos, D., Moreau, C., Devedjian, J.C., Kluza, J., Petrault, M., Laloux, C., Jonneaux, A., Ryckewaert, G., Garçon, G., Rouaix, N., et al. (2014). Targeting chelatable iron as a therapeutic modality in Parkinson's disease. Antioxid. Redox Signal. *21*, 195–210.

Dexter, D.T., Wells, F.R., Agid, F., Agid, Y., Lees, A.J., Jenner, P., and Marsden, C.D. (1987). Increased nigral iron content in postmortem parkinsonian brain. Lancet *2*, 1219–1220.

Ding, H., Yan, C.Z., Shi, H., Zhao, Y.S., Chang, S.Y., Yu, P., Wu, W.S., Zhao, C.Y., Chang, Y.Z., and Duan, X.L. (2011). Hepcidin is involved in iron regulation in the ischemic brain. PLoS One *6*, e25324.

Du, F., Qian, C., Qian, Z.M., Wu, X.M., Xie, H., Yung, W.H., and Ke, Y. (2011). Hepcidin directly inhibits transferrin receptor 1 expression in astrocytes via a cyclic AMP-protein kinase A pathway. Glia *59*, 936–945.

Du, F., Qian, Z., Luo, Q., Yung, W., and Ke, Y. (2015). Hepcidin suppresses brain iron accumulation by downregulating iron transport proteins in iron-overloaded rats. Mol. Neurobiol. *52*, 101–114.

Du, F., Qian, Z.M., Gong, Q., Zhu, Z.J., Lu, L., and Ke, Y. (2012). The iron regulatory hormone hepcidin inhibits expression of iron release as well as iron uptake proteins in J774 cells. J. Nutr. Biochem. *23*, 1694–1700.

Ebrahimi-Fakhari, D., Cantuti-Castelvetri, I., Fan, Z., Rockenstein, E., Masliah, E., Hyman, B.T., McLean, P.J., and Unni, V.K. (2011). Distinct roles in vivo for the ubiquitin-proteasome system and the autophagy-lysosomal pathway in the degradation of alpha-synuclein. J. Neurosci. *31*, 14508–14520.

Ebrahimi-Fakhari, D., Wahlster, L., and McLean, P.J. (2012). Protein degradation pathways in Parkinson's disease: curse or blessing. Acta Neuropathol. *124*, 153–172.

Elkouzi, A., Vedam-Mai, V., Eisinger, R.S., and Okun, M.S. (2019). Emerging therapies in Parkinson disease - repurposed drugs and new approaches. Nat. Rev. Neurol. *15*, 204–223.

Feng, Y., Liang, Z.H., Wang, T., Qiao, X., Liu, H.J., and Sun, S.G. (2006). alpha-Synuclein redistributed and aggregated in rotenone-induced Parkinson's disease rats. Neurosci. Bull. *22*, 288–293.

Finkelstein, D., Billings, J., Adlard, P., Ayton, S., Sedjahtera, A., Masters, C., Wilkins, S., Shackleford, D., Charman, S., Bal, W., et al. (2017). The novel compound PBT_{434} prevents iron mediated neurodegeneration and alpha-synuclein toxicity in multiple models of Parkinsons disease. Acta Neuropathol. Commun. *5*, 53.

Fujiwara, H., Hasegawa, M., Dohmae, N., Kawashima, A., Masliah, E., Goldberg, M.S., Shen, J., Takio, K., and Iwatsubo, T. (2002). alpha-Synuclein is phosphorylated in synucleinopathy lesions. Nat. Cell Biol. *4*, 160–164.

Ganguly, U., Banerjee, A., Chakrabarti, S.S., Kaur, U., Sen, O., Cappai, R., and Chakrabarti, S. (2020). Interaction of α-synuclein and Parkin in iron toxicity on SH-SY5Y cells: implications in the pathogenesis of Parkinson's disease. Biochem. J. *477*, 1109–1122.

Gelders, G., Baekelandt, V., and Van der Perren, A. (2018). Linking neuroinflammation and neurodegeneration in Parkinson's disease. J. Immunol. Res. *2018*, 4784268.

Geto, Z., Molla, M.D., Challa, F., Belay, Y., and Getahun, T. (2020). Mitochondrial dynamic dysfunction as a main triggering factor for inflammation associated chronic non-communicable diseases. J. Inflamm. Res. *13*, 97–107.

Ghassaban, K., He, N., Sethi, S.K., Huang, P., Chen, S., Yan, F., and Haacke, E.M. (2019). Regional high iron in the substantia nigra differentiates Parkinson's disease patients from healthy controls. Front Aging Neurosci. *11*, 106.

Goedert, M. (2015). Neurodegeneration. Alzheimer's and Parkinson's diseases: the prion concept in relation to assembled Aβ, tau, and α-synuclein. Science *349*, 1255555.

Gong, J., Du, F., Qian, Z.M., Luo, Q.Q., Sheng, Y., Yung, W.H., Xu, Y.X., and Ke, Y. (2016). Pre-treatment of rats with ad-hepcidin prevents iron-induced oxidative stress in the brain. Free Radic. Biol. Med. *90*, 126–132.

Gonzalez, H., and Pacheco, R. (2014). T-cell-mediated regulation of neuroinflammation involved in neurodegenerative diseases. J. Neuroinflamm. *11*, 201.

Grabrucker, A.M., Ruozi, B., Belletti, D., Pederzoli, F., Forni, F., Vandelli, M.A., and Tosi, G. (2016). Nanoparticle transport across the blood brain barrier. Tissue Barriers *4*, e1153568.

Grassi, D., Howard, S., Zhou, M., Diaz-Perez, N., Urban, N.T., Guerrero-Given, D., Kamasawa, N., Volpicelli-Daley, L.A., Lograsso, P., and Lasmezas, C.I. (2018). Identification of a highly neurotoxic alpha-synuclein species inducing mitochondrial damage and mitophagy in Parkinson's disease. Proc. Natl. Acad. Sci. U S A *115*, e2634–e2643.

Grivennikova, V.G., Maklashina, E.O., Gavrikova, E.V., and Vinogradov, A.D. (1997). Interaction of the mitochondrial NADH-ubiquinone reductase with rotenone as related to the enzyme active/inactive transition. Biochim. Biophys. Acta *1319*, 223–232.

Grünewald, A., Kumar, K.R., and Sue, C.M. (2019). New insights into the complex role of mitochondria in Parkinson's disease. Prog. Neurobiol. *177*, 73–93.

Gutman, M., Singer, T.P., Beinert, H., and Casida, J.E. (1970). Reaction sites of rotenone, piericidin

A, and amytal in relation to the nonheme iron components of NADH dehydrogenase. Proc. Natl. Acad. Sci. U S A *65*, 763–770.

Hadzhieva, M., Kirches, E., and Mawrin, C. (2014). Review: iron metabolism and the role of iron in neurodegenerative disorders. Neuropathol. Appl. Neurobiol. *40*, 240–257.

Haelterman, N.A., Yoon, W.H., Sandoval, H., Jaiswal, M., Shulman, J.M., and Bellen, H.J. (2014). A mitocentric view of Parkinson's disease. Annu. Rev. Neurosci. *37*, 137–159.

Hauser, D.N., and Hastings, T.G. (2013). Mitochondrial dysfunction and oxidative stress in Parkinson's disease and monogenic parkinsonism. Neurobiol. Dis. *51*, 35–42.

Hentze, M.W., Muckenthaler, M.U., Galy, B., and Camaschella, C. (2010). Two to tango: regulation of Mammalian iron metabolism. Cell *142*, 24–38.

Hirsch, E.C., Brandel, J.P., Galle, P., Javoy-Agid, F., and Agid, Y. (1991). Iron and aluminum increase in the substantia nigra of patients with Parkinson's disease: an X-ray microanalysis. J. Neurochem. *56*, 446–451.

Hou, Y.S., Guan, J.J., Xu, H.D., Wu, F., Sheng, R., and Qin, Z.H. (2015). Sestrin2 protects dopaminergic cells against rotenone toxicity through AMPK-dependent autophagy activation. Mol. Cell. Biol. *35*, 2740–2751.

Jang, W., Kim, H.J., Li, H., Jo, K.D., Lee, M.K., and Yang, H.O. (2016). The neuroprotective effect of erythropoietin on rotenone-induced neurotoxicity in SH-SY5Y cells through the induction of autophagy. Mol. Neurobiol. *53*, 3812–3821.

Jia, W., Xu, H., Du, X., Jiang, H., and Xie, J. (2015). Ndfip1 attenuated 6-OHDA-induced iron accumulation via regulating the degradation of DMT1. Neurobiol. Aging *36*, 1183–1193.

Jiang, H., Song, N., Jiao, Q., Shi, L., and Du, X. (2019). Iron pathophysiology in Parkinson diseases. Adv. Exp. Med. Biol. *1173*, 45–66.

Jiang, H., Song, N., Xu, H., Zhang, S., Wang, J., and Xie, J. (2010). Up-regulation of divalent metal transporter 1 in 6-hydroxydopamine intoxication is IRE/IRP dependent. Cell Res. *20*, 345–356.

Joppe, K., Roser, A.E., Maass, F., and Lingor, P. (2019). The contribution of iron to protein aggregation disorders in the central nervous system. Front Neurosci. *13*, 15.

Kahle, P.J., Neumann, M., Ozmen, L., Muller, V., Odoy, S., Okamoto, N., Jacobsen, H., Iwatsubo, T., Trojanowski, J.Q., Takahashi, H., et al. (2001). Selective insolubility of alpha-synuclein in human Lewy body diseases is recapitulated in a transgenic mouse model. Am. J. Pathol. *159*, 2215–2225.

Kalia, L.V., Kalia, S.K., McLean, P.J., Lozano, A.M., and Lang, A.E. (2013). α-Synuclein oligomers and clinical implications for Parkinson disease. Ann. Neurol. *73*, 155–169.

Kaur, D., Yantiri, F., Rajagopalan, S., Kumar, J., Mo, J.Q., Boonplueang, R., Viswanath, V., Jacobs, R., Yang, L., Beal, M.F., et al. (2003). Genetic or pharmacological iron chelation prevents MPTP-induced neurotoxicity in vivo: a novel therapy for Parkinson's disease. Neuron *37*, 899–909.

Kostka, M., Hogen, T., Danzer, K.M., Levin, J., Habeck, M., Wirth, A., Wagner, R., Glabe, C.G., Finger, S., Heinzelmann, U., et al. (2008). Single particle characterization of iron-induced pore-forming alpha-synuclein oligomers. J. Biol. Chem. *283*, 10992–11003.

Kustrimovic, N., Marino, F., and Cosentino, M. (2019). Peripheral immunity, immunoaging and neuroinflammation in Parkinson's disease. Curr. Med. Chem. *26*, 3719–3753.

Langley, J., He, N., Huddleston, D.E., Chen, S., Yan, F., Crosson, B., Factor, S., and Hu, X. (2019). Reproducible detection of nigral iron deposition in 2 Parkinson's disease cohorts. Mov. Disord. *34*, 416–419.

Lee, D.W., Rajagopalan, S., Siddiq, A., Gwiazda, R., Yang, L., Beal, M.F., Ratan, R.R., and Andersen, J.K. (2009). Inhibition of prolyl hydroxylase protects against 1-methyl-4-phenyl-1,2,3,6-tetrahydropyridine-induced neurotoxicity: model for the potential involvement of the hypoxia-inducible factor pathway in Parkinson disease. J. Biol. Chem. *284*, 29065–29076.

Lee, M.K., Stirling, W., Xu, Y., Xu, X., Qui, D., Mandir, A.S., Dawson, T.M., Copeland, N.G., Jenkins, N.A., and Price, D.L. (2002). Human alpha-synuclein-harboring familial Parkinson's disease-linked Ala-53–> Thr mutation causes neurodegenerative disease with alpha-synuclein aggregation in transgenic mice. Proc. Natl. Acad. Sci. U S A *99*, 8968–8973.

Levi, S., Corsi, B., Bosisio, M., Invernizzi, R., Volz, A., Sanford, D., Arosio, P., and Drysdale, J. (2001). A human mitochondrial ferritin encoded by an intronless gene. J. Biol. Chem. *276*, 24437–24440.

Levin, J., Hogen, T., Hillmer, A.S., Bader, B., Schmidt, F., Kamp, F., Kretzschmar, H.A., Botzel, K., and Giese, A. (2011). Generation of ferric iron links oxidative stress to alpha-synuclein oligomer formation. J. Parkinsons Dis. *1*, 205–216.

Li, W.J., Jiang, H., Song, N., and Xie, J.X. (2010). Dose- and time-dependent alpha-synuclein aggregation induced by ferric iron in SK-N-SH cells. Neurosci. Bull. *26*, 205–210.

Liddell, J.R., and White, A.R. (2018). Nexus between mitochondrial function, iron, copper and glutathione in Parkinson's disease. Neurochem. Int. *117*, 126–138.

Lonskaya, I., Hebron, M.L., Algarzae, N.K., Desforges, N., and Moussa, C.E. (2013). Decreased parkin solubility is associated with impairment of autophagy in the nigrostriatum of sporadic Parkinson's disease. Neuroscience *232*, 90–105.

Lv, Z., Jiang, H., Xu, H., Song, N., and Xie, J. (2011). Increased iron levels correlate with the selective nigral dopaminergic neuron degeneration in Parkinson's disease. J. Neural Transm. *118*, 361–369.

Mastroberardino, P.G., Hoffman, E.K., Horowitz, M.P., Betarbet, R., Taylor, G., Cheng, D., Na, H.M., Gutekunst, C.A., Gearing, M., Trojanowski, J.Q., et al. (2009). A novel transferrin/TfR2-mediated mitochondrial iron transport system is disrupted in Parkinson's disease. Neurobiol. Dis. *34*, 417–431.

Matak, P., Matak, A., Moustafa, S., Aryal, D.K., Benner, E.J., Wetsel, W., and Andrews, N.C. (2016). Disrupted iron homeostasis causes dopaminergic neurodegeneration in mice. Proc. Natl. Acad. Sci. U S A *113*, 3428–3435.

McCarthy, R.C., and Kosman, D.J. (2014). Glial cell ceruloplasmin and hepcidin differentially regulate iron efflux from brain microvascular endothelial cells. PLoS One *9*, e89003.

Mena, N.P., Bulteau, A.L., Salazar, J., Hirsch, E.C., and Núñez, M.T. (2011). Effect of mitochondrial complex I inhibition on Fe–S cluster protein activity. Biochem. Biophys. Res. Commun. *409*, 241–246.

Mena, N.P., Garcia-Beltran, O., Lourido, F., Urrutia, P.J., Mena, R., Castro-Castillo, V., Cassels, B.K., and Nunez, M.T. (2015a). The novel mitochondrial iron chelator 5-((methylamino) methyl)-8-hydroxyquinoline protects against mitochondrial-induced oxidative damage and neuronal death. Biochem. Biophys. Res. Commun. *463*, 787–792.

Mena, N.P., Urrutia, P.J., Lourido, F., Carrasco, C.M., and Núñez, M.T. (2015b). Mitochondrial iron homeostasis and its dysfunctions in neurodegenerative disorders. Mitochondrion *21*, 92–105.

Moreau, C., Duce, J.A., Rascol, O., Devedjian, J.C., Berg, D., Dexter, D., Cabantchik, Z.I., Bush, A.I., and Devos, D. (2018). Iron as a therapeutic target for Parkinson's disease. Mov. Disord. *33*, 568–574.

Mouhape, C., Costa, G., Ferreira, M., Abin-Carriquiry, J.A., Dajas, F., and Prunell, G. (2019). Nicotine-induced neuroprotection in rotenone in vivo and in vitro models of Parkinson's disease: evidences for the involvement of the labile iron pool level as the underlying mechanism. Neurotox Res. *35*, 71–82.

Mracsko, E., and Veltkamp, R. (2014). Neuroinflammation after intracerebral hemorrhage. Front. Cell Neurosci. *8*, 388.

Muñoz, Y., Carrasco, C.M., Campos, J.D., Aguirre, P., and Núñez, M.T. (2016). Parkinson's disease: the mitochondria-iron link. Parkinsons Dis. *2016*, 7049108.

Murriel, C.L., and Dowdy, S.F. (2006). Influence of protein transduction domains on intracellular delivery of macromolecules. Expert Opin. Drug Deliv. *3*, 739–746.

Nuñez, M.T., and Chana-Cuevas, P. (2018). New perspectives in iron chelation therapy for the treatment of neurodegenerative diseases. Pharmaceuticals (Basel) *11*, 109.

Pardridge, W.M. (2015). Blood–brain barrier drug delivery of IgG fusion proteins with a transferrin receptor monoclonal antibody. Expert Opin. Drug Deliv. *12*, 207–222.

Peng, Y., Wang, C., Xu, H.H., Liu, Y.N., and Zhou, F. (2010). Binding of alpha-synuclein with Fe(III) and with Fe(II) and biological implications of the resultant complexes. J. Inorg. Biochem. *104*, 365–370.

Petrat, F., Weisheit, D., Lensen, M., De Groot, H., Sustmann, R., and Rauen, U. (2002). Selective determination of mitochondrial chelatable iron in viable cells with a new fluorescent sensor. Biochem. J. *362*, 137–147.

Pyatigorskaya, N., Sharman, M., Corvol, J.C., Valabregue, R., Yahia-Cherif, L., Poupon, F., Cormier-Dequaire, F., Siebner, H., Klebe, S., Vidailhet, M., et al. (2015). High nigral iron deposition in LRRK2 and Parkin mutation carriers using R2* relaxometry. Mov. Disord. *30*, 1077–1084.

Qian, Z.M., and Ke, Y. (2019). Hepcidin and its therapeutic potential in neurodegenerative disorders. Med. Res. Rev. *40*, 633–653.

Raha-Chowdhury, R., Raha, A.A., Forostyak, S., Zhao, J.W., Stott, S.R., and Bomford, A. (2015). Expression and cellular localization of hepcidin mRNA and protein in normal rat brain. BMC Neurosci. *16*, 24.

Raha, A.A., Vaishnav, R.A., Friedland, R.P., Bomford, A., and Raha-Chowdhury, R. (2013). The systemic iron-regulatory proteins hepcidin and ferroportin are reduced in the brain in Alzheimer's disease. Acta Neuropathol. Commun. *1*, 55.

Ramsay, R.R., and Singer, T.P. (1992). Relation of superoxide generation and lipid peroxidation to the inhibition of NADH-Q oxidoreductase by rotenone, piericidin A, and MPP+. Biochem. Biophys. Res. Commun. *189*, 47–52.

Rauen, U., Kerkweg, U., Weisheit, D., Petrat, F., Sustmann, R., and De Groot, H. (2003). Cold-induced apoptosis of hepatocytes: mitochondrial permeability transition triggered by nonmitochondrial chelatable iron. Free Radic. Biol. Med. *35*, 1664–1678.

Rosset, M.B., Lui, G., Dansokho, C., Chaigneau, T., and Dorothee, G. (2015). Vaccine-induced Aβ-specific CD8+ T cells do not trigger autoimmune neuroinflammation in a murine model of Alzheimer's disease. J. Neuroinflam. *12*, 95.

Salazar, J., Mena, N., Hunot, S., Prigent, A., Alvarez-Fischer, D., Arredondo, M., Duyckaerts, C., Sazdovitch, V., Zhao, L., Garrick, L.M., et al. (2008). Divalent metal transporter 1 (DMT1) contributes to neurodegeneration in animal models of Parkinson's disease. Proc. Natl. Acad. Sci. U S A *105*, 18578–18583.

Shachar, D.B., Kahana, N., Kampel, V., Warshawsky, A., and Youdim, M.B. (2004). Neuroprotection by a novel brain permeable iron chelator, VK-28, against 6-hydroxydopamine lession in rats. Neuropharmacology *46*, 254–263.

Shi, Z.H., Nie, G., Duan, X.L., Rouault, T., Wu, W.S., Ning, B., Zhang, N., Chang, Y.Z., and Zhao, B.L. (2010). Neuroprotective mechanism of mitochondrial ferritin on 6-hydroxydopamine-induced dopaminergic cell damage: implication for neuroprotection in Parkinson's disease. Antioxid. Redox Signal. *13*, 783–796.

Singh, Y.P., Pandey, A., Vishwakarma, S., and Modi, G. (2019). A review on iron chelators as potential therapeutic agents for the treatment of Alzheimer's and Parkinson's diseases. Mol. Divers. *23*, 509–526.

Solleiro-Villavicencio, H., and Rivasarancibia, S. (2018). Effect of chronic oxidative stress on neuroinflammatory response mediated by CD4+T cells in neurodegenerative diseases. Front. Cell Neurosci. *12*, 114.

Song, N., Jiang, H., Wang, J., and Xie, J.X. (2007). Divalent metal transporter 1 up-regulation is involved in the 6-hydroxydopamine-induced ferrous iron influx. J. Neurosci. Res. *85*, 3118–3126.

Song, N., Wang, J., Jiang, H., and Xie, J. (2010). Ferroportin 1 but not hephaestin contributes to iron accumulation in a cell model of Parkinson's disease. Free Radic. Biol. Med. *48*, 332–341.

Spillantini, M.G., Schmidt, M.L., Lee, V.M.Y., Trojanowski, J.Q., Jakes, R., and Goedert, M. (1997). α-Synuclein in Lewy bodies. Nature *388*, 839–840.

Stephenson, J., Nutma, E., Van der Valk, P., and Amor, S. (2018). Inflammation in CNS neurodegenerative diseases. Immunology *154*, 204–219.

Stolp, H.B., and Dziegielewska, K.M. (2009). Review: role of developmental inflammation and blood-brain barrier dysfunction in neurodevelopmental and neurodegenerative diseases. Neuropathol. Appl. Neurobiol. *35*, 132–146.

Tan, G., Liu, L., He, Z., Sun, J., Xing, W., and Sun, X. (2016). Role of hepcidin and its downstream proteins in early brain injury after experimental subarachnoid hemorrhage in rats. Mol. Cell. Biochem. *418*, 31–38.

Thomas, G.E.C., Leyland, L.A., Schrag, A.E., Lees, A.J., Acosta-Cabronero, J., and Weil, R.S. (2020). Brain iron deposition is linked with cognitive severity in Parkinson's disease. J. Neurol. Neurosurg. Psychiatry *91*, 418–425.

Troncosoescudero, P., Parra, A.V., Nassif, M., and Vidal, R.L. (2018). Outside in: unraveling the role of neuroinflammation in the progression of Parkinson's disease. Front. Neurol. *9*, 860.

Trudler, D., Nash, Y., and Frenkel, D. (2015). New insights on Parkinson's disease genes: the link between mitochondria impairment and neuroinflammation. J. Neural Transm. *122*, 1409–1419.

Urrutia, P.J., Aguirre, P., Tapia, V., Carrasco, C.M., Mena, N.P., and Núñez, M.T. (2017a). Cell death induced by mitochondrial complex I inhibition is mediated by Iron Regulatory Protein 1. Biochim. Biophys. Acta Mol. Basis Dis. *1863*, 2202–2209.

Urrutia, P.J., Hirsch, E.C., González-Billault, C., and Núñez, M.T. (2017b). Hepcidin attenuates amyloid beta-induced inflammatory and pro-oxidant responses in astrocytes and microglia. J. Neurochem. *142*, 140–152.

Urrutia, P.J., Mena, N.P., and Núñez, M.T. (2014). The interplay between iron accumulation, mitochondrial dysfunction, and inflammation during the execution step of neurodegenerative disorders. Front. Pharmacol. *5*, 38.

Vela, D. (2018). The dual role of hepcidin in brain iron load and inflammation. Front Neurosci. *12*, 740.

Wang, B., and Wang, X.-P. (2019). Does ceruloplasmin defend against neurodegenerative diseases? Curr. Neuropharmacol. *17*, 539–549.

Wang, X., Xuan, W., Zhu, Z.Y., Li, Y., Zhu, H., Zhu, L., Fu, D.Y., Yang, L.Q., Li, P.Y., and Yu, W.F. (2018). The evolving role of neuro-immune interaction in brain repair after cerebral ischemic stroke. CNS Neurosci. Ther. *24*, 1100–1114.

Workman, D.G., Tsatsanis, A., Lewis, F.W., Boyle, J.P., Mousadoust, M., Hettiarachchi, N.T., Hunter, M., Peers, C.S., Tetard, D., and Duce, J.A. (2015). Protection from neurodegeneration in the 6-hydroxydopamine (6-OHDA) model of Parkinson's with novel 1-hydroxypyridin-2-one metal chelators. Metallomics *7*, 867–876.

Wu, G., Pang, S., Feng, X., Zhang, A., Li, J., Gu, K., Huang, J., Dong, H., and Yan, B. (2011). Genetic analysis of lysosomal alpha-galactosidase A gene in sporadic Parkinson's disease. Neurosci. Lett. *500*, 31–35.

Wu, Y., Li, X., Xie, W., Jankovic, J., Le, W., and Pan, T. (2010). Neuroprotection of deferoxamine on rotenone-induced injury via accumulation of HIF-1 alpha and induction of autophagy in SH-SY5Y cells. Neurochem. Int. *57*, 198–205.

Xiong, X.Y., Liu, L., Wang, F.X., Yang, Y.R., Hao, J.W., Wang, P.F., Zhong, Q., Zhou, K., Xiong, A., Zhu, W.Y., et al. (2016). Toll-like receptor 4/MyD88-mediated signaling of hepcidin expression causing brain iron accumulation, oxidative injury, and cognitive impairment after intracerebral hemorrhage. Circulation *134*, 1025–1038.

Xu, Q., Langley, M., Kanthasamy, A.G., and Reddy, M.B. (2017). Epigallocatechin gallate has a neurorescue effect in a mouse model of Parkinson disease. J. Nutr. *147*, 1926–1931.

You, L.H., Li, Z., Duan, X.L., Zhao, B.L., Chang, Y.Z., and Shi, Z.H. (2016). Mitochondrial ferritin suppresses MPTP-induced cell damage by regulating iron metabolism and attenuating oxidative stress. Brain Res. *1642*, 33–42.

Zhang, S., Wang, J., Song, N., Xie, J., and Jiang, H. (2009). Up-regulation of divalent metal transporter 1 is involved in 1-methyl-4-phenylpyridinium (MPP(+))-induced apoptosis in MES23.5 cells. Neurobiol. Aging *30*, 1466–1476.

Zhang, Z., Hou, L., Song, J.L., Song, N., Sun, Y.J., Lin, X., Wang, X.L., Zhang, F.Z., and Ge, Y.L. (2014). Pro-inflammatory cytokine-mediated ferroportin down-regulation contributes to the nigral iron accumulation in lipopolysaccharide-induced Parkinsonian models. Neuroscience *257*, 20–30.

Zhou, Y.F., Zhang, C., Yang, G., Qian, Z.M., Zhang, M.W., Ma, J., Zhang, F.L., and Ke, Y. (2017). Hepcidin protects neuron from hemin-mediated injury by reducing iron. Front Physiol. *8*, 332.

Zhu, T., Zhang, F., Li, H., He, Y., Zhang, G., Huang, N., Guo, M., and Li, X. (2019). Long-term icariin treatment ameliorates cognitive deficits via CD4 + T cell-mediated immuno-inflammatory responses in APP/PS1 mice. Clin. Interv. Aging *14*, 817–826.

iScience, Volume *23*

Supplemental Information

Brain Hepcidin Suppresses Major Pathologies in Experimental Parkinsonism

Tuo Liang, Zhong-Ming Qian, Ming-Dao Mu, Wing-Ho Yung, and Ya Ke

Supplemental figures and legends

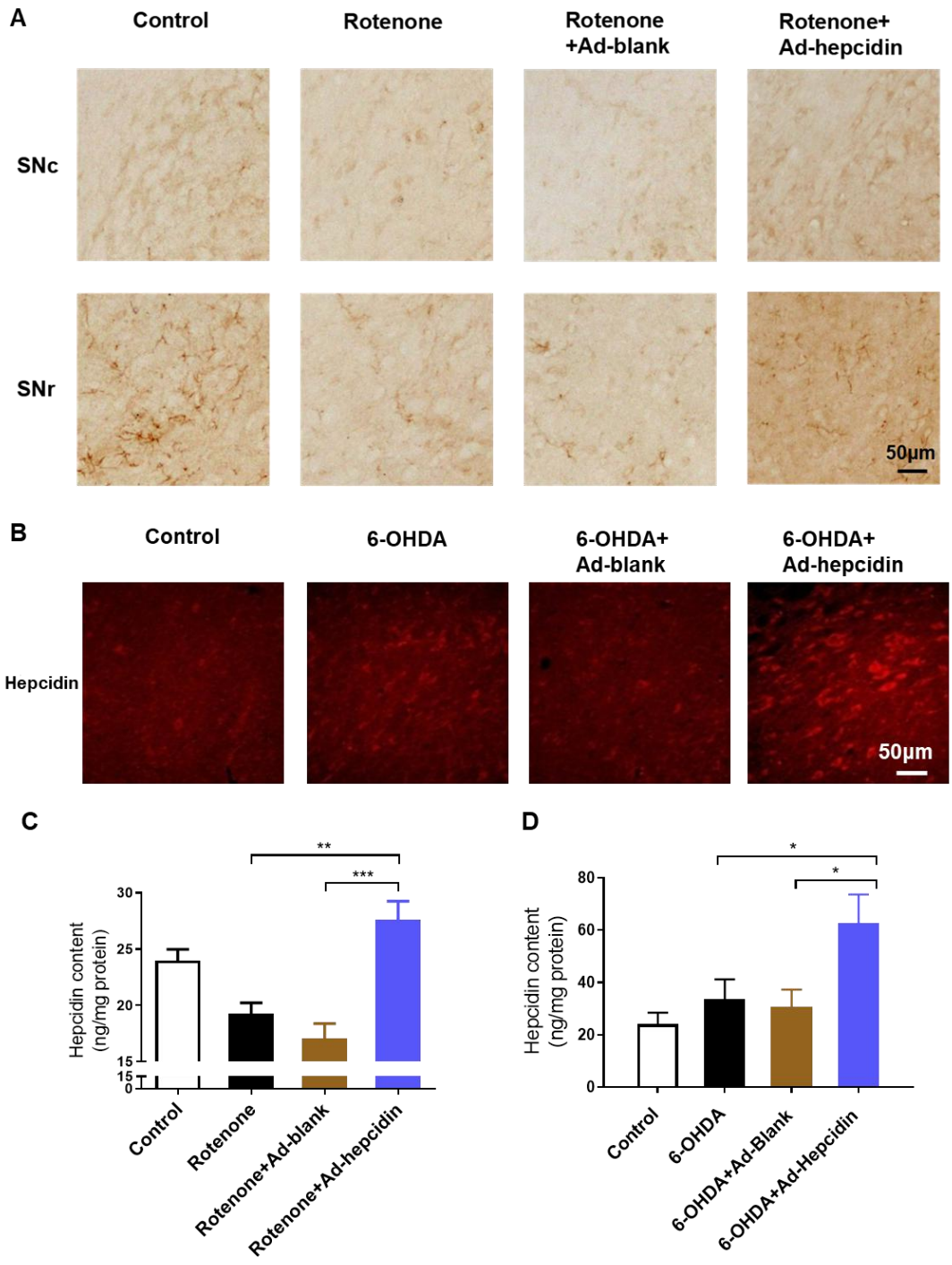

Supplementary Figure 1. Ad-hepcidin injection increased hepcidin levels in rotenone and 6-OHDA models of PD, related to Figure 1 Rotenone injection (IP) induced suppression of hepcidin both in the SNc and SNr, which was reversed by injection (ICV) of Ad-hepcidin but not Ad-blank, as detected by immunohistochemistry. The scale bar represents 50μm (A). Hepcidin levels in the SN were maintained in 6-OHDA-treated rats, while Ad-hepcidin increased hepcidin levels (B). The above observations were quantified by ELISA (C, D). * $P < 0.05$, ** $P < 0.01$, *** $P < 0.001$, one-way ANOVA (n=5-15 in each group); error bars, S.E.M..

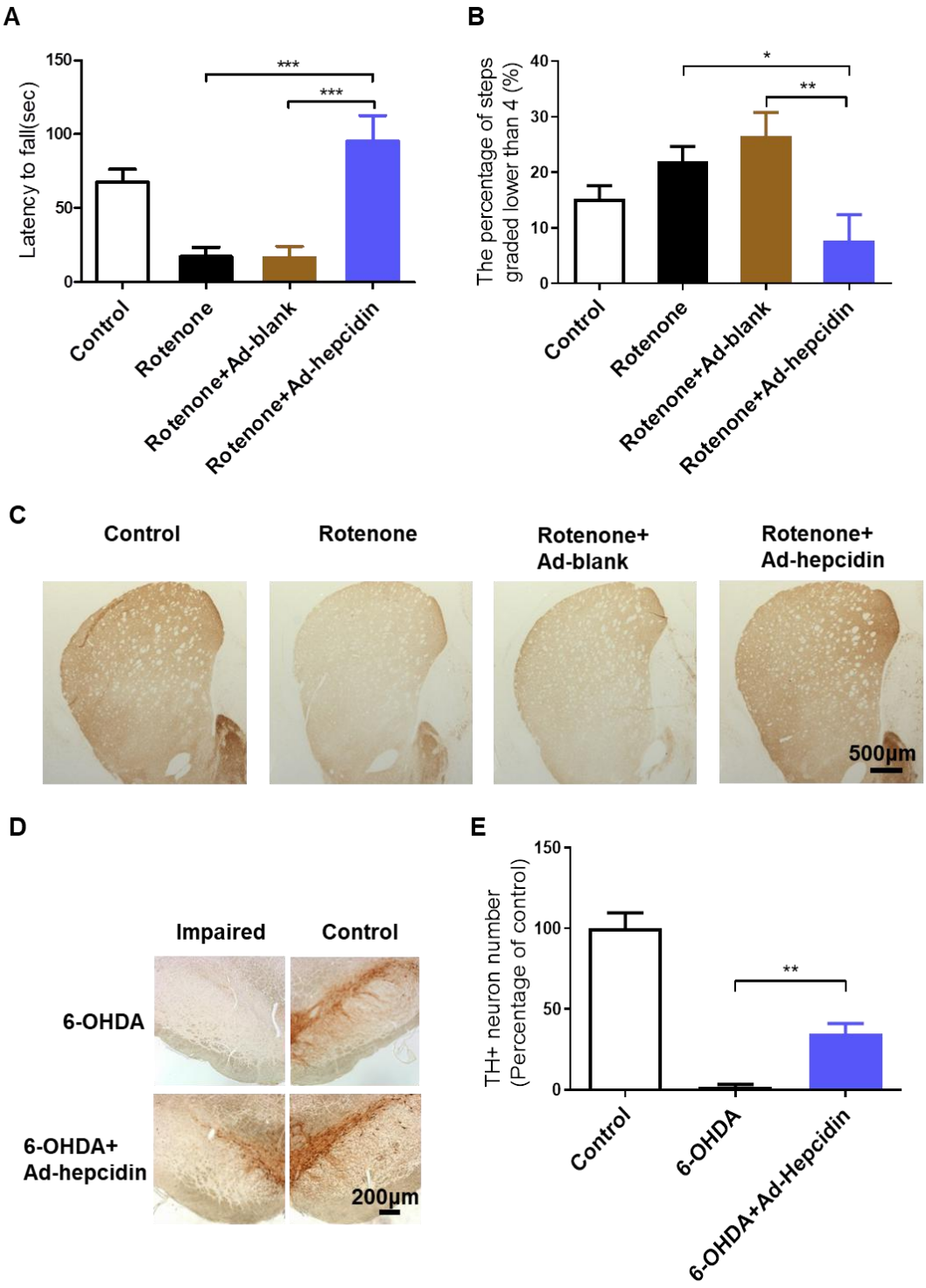

Supplementary Figure 2. Ad-hepcidin restored rotenone- and 6-OHDA-induced motor deficiency and TH$^+$ signal loss, related to Figure 1 Injection (IP) of rotenone dramatically decreased the time of animals stayed on the rotarod, while Ad-hepcidin injection (ICV) rescued these motor deficits (A). In the ladder rung walking test, each step was rated from 6 to 0 based on performance following standard criteria. The increased percentage of low-grade steps induced by rotenone was also suppressed by Ad-hepcidin (B). TH$^+$ signal was decreased in rotenone-treated rats in striatum, while Ad-hepcidin ameliorated the reduction, as detected by immunohistochemistry. The scale bar represents 500μm (C). 6-OHDA unilateral injection caused severe TH$^+$ neuronal loss in the SN. Ad-hepcidin injection suppressed the TH$^+$ neuronal loss. The scale bar represents 200μm (D). The statistical result of TH$^+$ neurons is presented as percentage of control (E). * $P < 0.05$, ** $P < 0.01$, *** $P < 0.001$, one-way ANOVA (n=5-15 in each group); error bars, S.E.M..

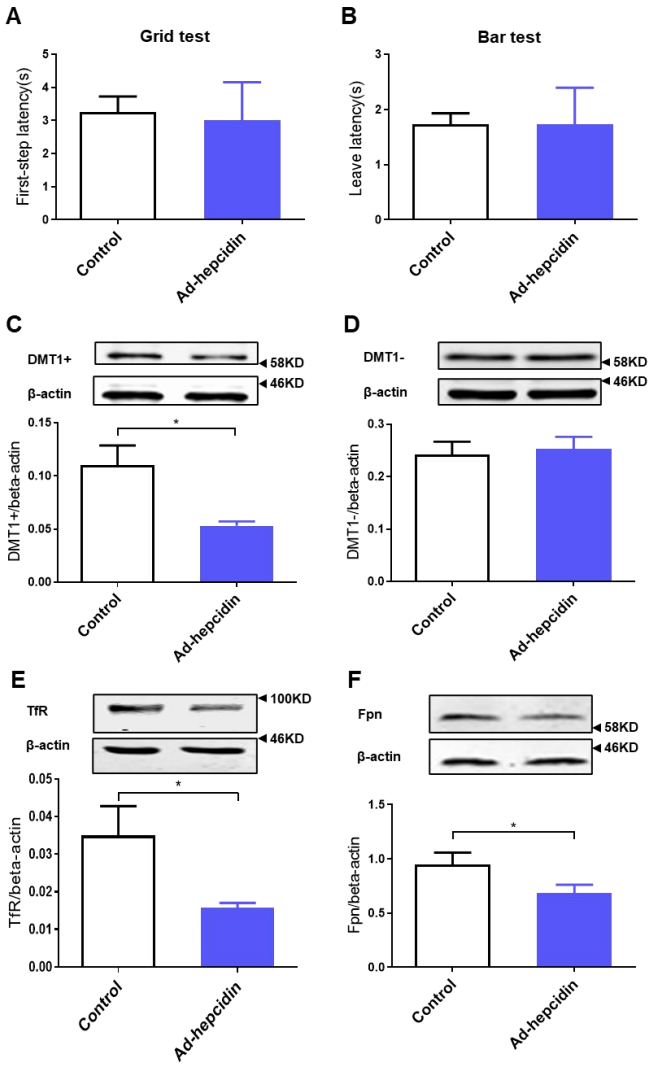

Supplementary Figure 3. Ad-hepcidin injection regulated iron-transport proteins without affecting motor ability in normal rats, related to Figure 2 Ad-hepcidin injection (ICV) did not affect first-step and descent latencies in grid and bar test respectively in healthy rats (A, B). DMT1+, TfR and Fpn were reduced in the SN in Ad-hepcidin-injected rats (C, E, F). The levels of DMT1- were not affected by Ad-hepcidin (D). * $P < 0.05$, two-tailed t-test (n=5-15 in each group); error bars, S.E.M..

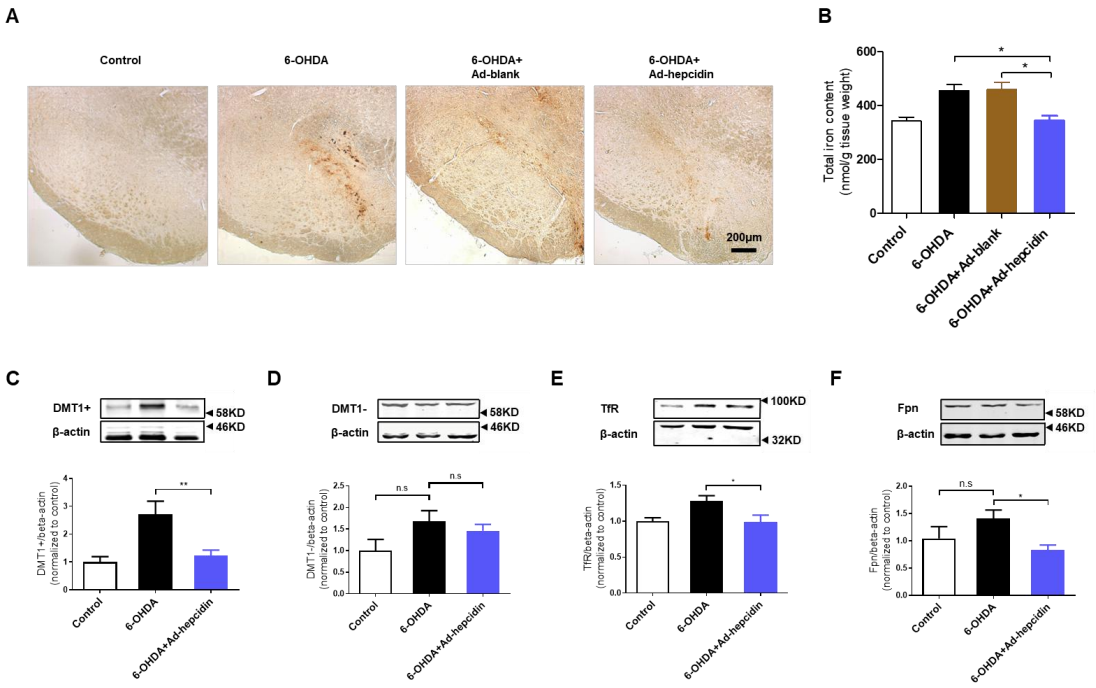

Supplementary Figure 4. Ad-hepcidin rectified 6-OHDA-induced iron accumulation and rotenone- and 6-OHDA- induced iron transport protein deregulation, related to Figure 2
Ad-hepcidin injection into SN suppressed iron accumulation in the SNc caused by 6-OHDA injection into the medial forebrain bundle. The scale bar represents 200μm (A). Ad-hepcidin also suppressed 6-OHDA-induced total iron increase in the SN (B). 6-OHDA injection induced an elevation of DMT1+ and TfR in the SN, while not affecting levels of DMT1- and Fpn (C, D, E, F). Ad-hepcidin injection significantly suppressed DMT1+, TfR and Fpn expression in the SN in 6-OHDA- injected rats, while not affecting DMT1- levels (C, D, E, F). * $P < 0.05$, ** $P < 0.01$, one-way ANOVA (n=5-10 for each group); n.s means no significance; error bar, S.E.M..

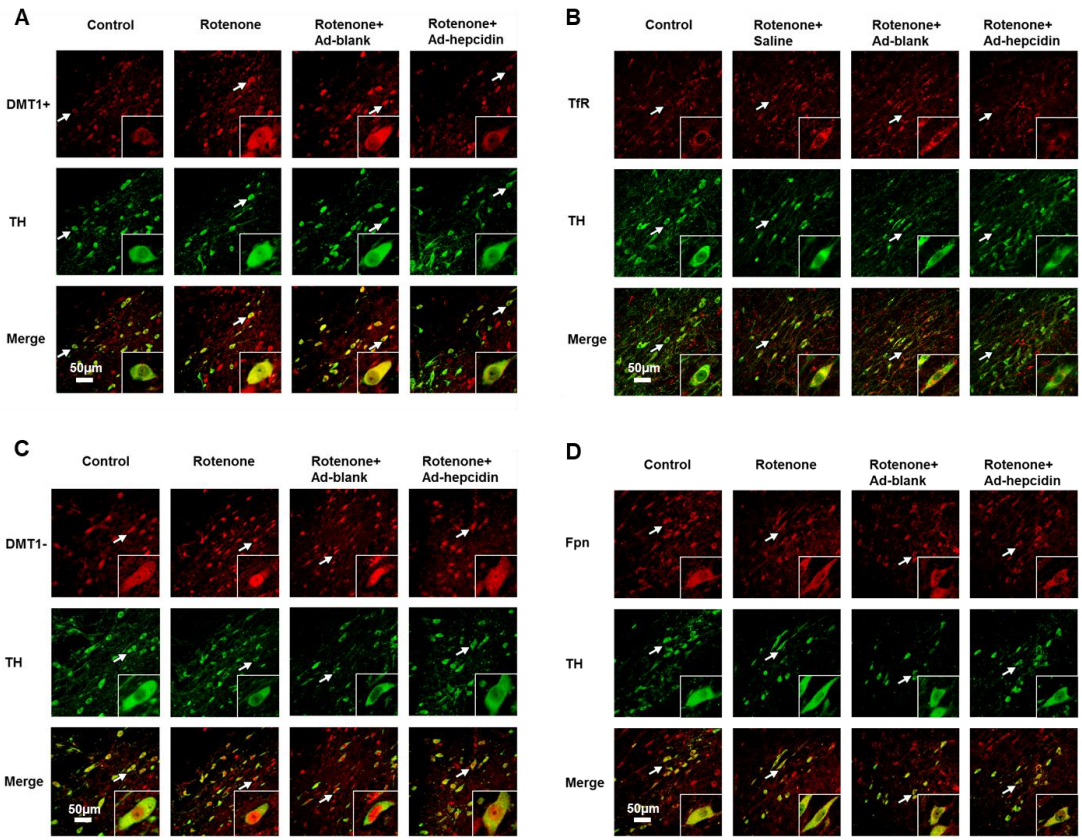

Supplementary Figure 5. Ad-hepcidin rectified rotenone-induced iron transport proteins dysregulation, related to Figure 2 Rotenone treatment (IP) caused DMT1+, TfR overexpression and DMT1- translocation in TH^+ neurons in the SNc, which was rectified by Ad-hepcidin injection (ICV) (A, B, C). Fpn expression in TH^+ neurons was slightly reduced by Ad-hepcidin (D). The scale bars represent 50μm.

Transparent Methods

Experimental model and subject details

Male Sprague–Dawley (SD) rats (3-month old) were obtained from the animal center of The Chinese University of Hong Kong and housed in an air-conditioned room that was kept at constant temperature and humidity in a 12-h light–dark cycle. Water and food were supplied ad libitum. The Animal Ethics and Experimentation Committee of the Chinese University of Hong Kong approved the use of animals for this study, and all experiments obey the relevant regulatory standards. The human neuroblastoma SH-SY5Y cell line was obtained from the Institute of Biochemistry and Cell Biology, Chinese Academy of Sciences (Shanghai, China). The cells were maintained in a 1:1 mixture of Dulbecco's modified Eagle's medium/Ham's F12 (Gibco, USA) and F-12 Nutrient Mixture (Ham12) (Gibco, USA) supplemented with 10 % fetal bovine serum (Gibco, USA), 100 mg/ml streptomycin (Gibco, USA), and 100 units/ml penicillin in a humidified atmosphere of 5 % CO_2 incubator at 37 °C.

Method details

Chemicals

Unless otherwise stated, all chemicals were obtained from the Sigma Chemical Company, St. Louis, MO, USA. Synthetic human hepcidin peptide (25 amino acids) was obtained from Peptides International, Louisville, KY,

USA.

PD animal models

SD rats were utilized to generate two animal models of PD in this study. A chronic rotenone model of PD was produced by intraperitoneal (IP) injection of rotenone, at a dose of 2.5 mg/kg daily for 35 days. 5 days after the start of rotenone injection, rats received an intracerebroventricular (ICV) administration of Ad-hepcidin, Ad-blank or vehicle at the following coordinates: 0.8 mm posterior to the bregma, 1.5 mm lateral to the midline. After rotenone injection for 35 days, behavioral tests were performed to assess motor ability. Then, rats were sacrificed for tissue sampling and analyses. A 6-OHDA model of PD in rats was produced by unilateral injection of 4 μg 6-OHDA into the medial forebrain bundle at 4.4 mm posterior to the bregma, 1.5 mm lateral to the midline. Rats also received an SN administration of Ad-hepcidin or vehicle at the following coordinates: 4.8 mm posterior to the bregma, 2.1 mm lateral to the midline. After 6-OHDA was injected for 14 days, cylinder test was performed to assess motor ability. Then, some rats were kept for 14 more days for testing apomorphine-induced rotation and TH staining, the others were sacrificed for all the other experiments.

Behavioral tests

The catalepsy test, stepping test, rotarod test and ladder rung walking test were performed 35 days after the start of rotenone injection to assess the motor ability of rats in different groups. The catalepsy test consisted of the grid test and the bar test (Huang et al., 2006, Bashkatova et al., 2004). In the grid test, the rat was made to hang from a vertical grid with a distance of 1 cm

between each wire. The time from holding onto the grid to the first paw movement was recorded as first-step latency. In the bar test, the forepaws of rat were placed on a bar parallel to and 5 cm above the base. The time from placing the front paws on the bar to the removal of one paw from the bar was recorded as the leave latency. In the stepping test (Olsson et al., 1995), the rat was held by the experimenter with one hand fixing the hindlimbs and slightly raising the animals' hind above the surface while the experimenter's other hand fixed the forelimb. With one paw touching the table, the rat was moved slowly sideways (5 sec for 0.9 m) by the experimenter, first forward and then in the backward. The number of adjusting steps was counted for both paws in the back and forward directions of movement. In the rotarod test (Li et al., 2017), rats were placed on a spinning roller, accelerating from 4 to 40 rpm at a rate of 20 rpm/min. The duration that each rat stayed on the rod was recorded and the maximum of testing time was 180 sec. Each rat was assessed for 5 times and the averaged latency was calculated to represent its motor ability. The ladder rung walking test was used to assess skilled walking in rats (Metz and Whishaw, 2009). The apparatus consisted of 2 walls and metal rungs (3 mm in diameter) that could be inserted to create a floor with a minimum distance of 1 cm between rungs. The pattern of the rungs was irregular and varied in different trials. The distance of the rungs changed randomly from 1 to 3 cm. Rats were trained to walk across the ladder for 5 times and then tested 5 times. The performance of limb placement was rated from 6 (best) to 0 (worst) as previously described. The cylinder test and apomorphine-induced rotation were also utilized to assess the motor deficits in the 6-OHDA induced model of PD (Rumpel et al., 2015). In cylinder test, rats were placed in a transparent cylinder for 3 min. The number of independent wall placements for the left

forelimb, right forelimb and both forelimbs simultaneously were counted in the cylinder, and the percentage of impaired forelimb use calculated. After subcutaneous injection of apomorphine (0.5 mg/kg), contralateral rotation was recorded for 15 min.

Virus construction

Hepcidin protein encoding region (GenBank NM-053469) was cloned, digested with BglII and SalI (New England, USA) and ligated into a green fluorescent protein (GFP)-tagged pAdTrack shuttle vector (Invitrogen, USA) (Du et al., 2015). The positive clone obtained (Hepc-shuttle), was transferred into Adeasy-1 plasmid containing BJ5183 E. coli. The positive clone (HepcAdeasy) was then linearized with Pac I (New England, USA) and transferred into HEK293 cells (Invitrogen, USA). One week later, recombinant viruses, named Ad-hepcidin, were collected and purified. GFP-expressing adenovirus, named Ad-blank, was utilized as negative control.

Cell treatment

For mitochondrial related experiments, cells were treated with 100nM rotenone for 1 day. For the other experiments, chronic cell model of PD was created by 20 nM rotenone treatment for 3 days to cause α-synuclein accumulation.

Immunohistochemistry

The fixed brain sections or cells were blocked with 4 % normal goat serum and incubated with diluted primary antibody. The sections were then washed and incubated with specific secondary antibody. For immunohistochemistry, antibody-incubated sections were washed and further immersed in a solution

containing DAB or VIP Peroxidase Substrate. The primary antibodies utilized for immunohistochemistry were: rabbit anti-tyrosine hydroxylase polyclonal antibody (Cat #AB152, Lot #1951919, EMD Millipore Corporation, Temecula, CA, USA); mouse anti-tyrosine hydroxylase antibody (Cat #MAB318, Lot #2585892, EMD Millipore Corporation, Temecula, CA, USA); mouse anti-TfR1 monoclonal antibody (Cat 13-6800, Invitrogen, Camarillo, USA); rabbit anti-DMT1+IRE, -DMT1-IRE polyclonal antibodies (Cat NRAMP21-S, Cat NRAMP23-S, Alpha Diagnostic International Inc, San Antonio, TX, USA); rabbit anti-ferroportin polyclonal antibodies(Cat MTP11-S, Alpha Diagnostic International Inc, TX, USA; Lot AIT001AN0102, Cat AIT-001, Alomone Labs, Jerusalem, Israel); mouse anti-α-synuclein antibody (Cat 610787, BD Biosciences, CA, USA). Secondary antibodies were Alexa 488/546 goat anti-rabbit/anti-mouse IgG (Invitrogen-Life Technologies, CA, USA) and goat anti-rabbit/mouse IgG-HRP antibody (Dako, Glostrup, Denmark).

Graphite furnace atomic absorption spectroscopy (GFAAS) total iron measurement

Homogenate of tissue/cell was added to a doubled volume of ultra-pure nitric acid and digested at 50°C for 48 hours. The standard curve was constructed by diluting iron standard. Both standards and samples were read by GFAAS machine (Perkin Elmer SIMAA 6000, Rautaruukki Ltd., Raahe, Finland). Iron absorbance was read at 248.3 nm, slit at 0.2 nm. The pretreatment temperature was 1400°C, and the atomization temperature was 2400°C.

Perls' iron staining

Perls' staining was utilized to detect the presence of iron in brain sections by

the insoluble Prussian blue dye, which is a complex hydrated ferric ferrocyanide substance (Meguro et al., 2007, Perls, 1867). Briefly, brain sections were incubated in a freshly prepared solution of 7% potassium ferrocyanide (3% HCl). After incubation, the sections were washed and immersed in 99 % methanol containing 1% hydrogen peroxide to quench endogenous peroxidase activity. Afterwards, the sections were washed and incubated in a solution of DAB to enhance the signals.

Western blot

Proteins from brain tissues or cultured cells were extracted with RIPA. Subsequently, the homogenates were centrifuged and the supernatants were harvested. For α-synuclein fractionation, brain tissues were lysated with triton, and pallets were further lysated with stronger detergent. The supernatants were denatured. Lysates were loaded and run in a single track of SDS-PAGE under reducing conditions and subsequently transferred to a pure nitrocellulose membrane. The blots were blocked and then incubated with primary antibodies. After that, the NC membrane was washed and incubated in appropriate secondary antibody. The primary antibody used: mouse anti-β-actin monoclonal antibody (Lot 052M4816V, Cat A2228, Sigma-Aldrich Inc). The primary antibodies used to detect TfR, DMT1+, DMT1-, Fpn and α-synculein in immunohistochemistry were also used for Western blot. The secondary antibodies: goat anti-mouse and anti-rabbit IRDye 800 CW IgG (Li-Cor, Lincoln, NE, USA).

Hepcidin measurements

Determinations of hepcidin contents in the SN were conducted with ELISA kits

(Shanghai Yuanye Bio-Technology Co., Ltd, China) following protocols provided by manufacturer.

Mitochondria isolation

Rats were decapitated and the brains were dissected out and chopped for mitochondria isolation (Sims and Anderson, 2008). Rat midbrains were transferred to Dounce homogenizer and isolation buffer was added to produce a 10 % mixture. The tissue pieces were homogenized and centrifuged at 1000g at 4℃ for 5 min. The supernatant was collected and centrifuged at 20000g at 4℃ for 10 min. The pellet was resuspended and homogenized in cold 15 % Percoll solution. The solution was pipetted on the upper layers of the density gradient (consisting of 23 % Percoll on the top and 40 % Percoll on the bottom in centrifuge tubes), and centrifuged at 30000g at 4℃ for 5 min. Then, the lowest band (enriched in mitochondria fraction) was collected. Isolation buffer was added to the mitochondrial fraction in a volume ratio of 4 : 1. The mixture was centrifuged at 16000g at 4℃ for 10 min. The pellet was added with fatty-acid-free BSA and isolation buffer and mixed gently. The mixture was centrifuged at 7000g at 4℃ for 10 min. The pellet was gently resuspended and homogenized in isolation buffer.

ATP measurement

Isolated mitochondria were immediately incubated for 5 min at 37℃ with 2.5 mM ADP, 1 mM pyruvate, and 1 mM malate. Luciferin substrate and luciferase enzyme (Promega, USA) were then added to generate luminescence. The bioluminescence was assessed on the Perkin Elmer Envision spectrophotometer. ATP in the SN were extracted by trichloroacetic acid and

measured using the same kit.

ROS production quantification

Isolated mitochondria were incubated for 30 min at 37°C in reaction buffer containing 10 μM H2-DCFDA. Fluorescence was read using a BMG Novo Star Galaxy spectrofluorimeter with 485 nm excitation and 520 nm emission filters.

Fluorimetric analysis of mitochondrial membrane potential (ΔΨm)

Isolated mitochondria or cultured cells were incubated with JC-1 staining buffer according to the manufacturer's instructions (Sigma, CS0760). The fluorescence intensity of JC-1 aggregate was detected with 520 nm excitation and 590 nm emission filters, whereas the JC-1 monomer was measured with 485 nm excitation and 520 nm emission filters using a BMG Novo Star Galaxy spectrofluorometer. The fluorescence intensity ratio of aggregates to monomers was calculated as an indicator of ΔΨm.

Complex I activity

The measurement has described in detail elsewhere (Estornell et al., 1993). Extracted mitochondria or the SN homogenate was reacted with a mixture containing CoQ and KCN at 37°C for 5min. Then, NADH was added and the absorbance was read at 340nm every 20sec for 2min to calculate the changing rate.

Transmission electron microscopy

Transmission electron microscopy was conducted to assess the morphological changes of mitochondria (Xu et al., 2015). Rats were quickly perfused with

saline followed by saline containing 0.5 % glutaraldehyde and 4 % paraformaldehyde. Samples of the SNc were further fixated in 2.5 % glutaraldehyde for 4 hours followed by 1-2 % osmium tetroxide for 45min. Then samples were dehydrated in graded alcohol. Afterwards, the pieces were washed with prophylene oxide, kept in prophylene oxide/Epon-812 mixture, and then embedded in Epon-812 resin for 2 days at 60°C. The embedded samples were sectioned at a thickness of 80 nm using a diamond knife (Diatome, Switzerland) on an Ultracut E microtome (Leica, Deerfield, IL). The sections were mounted on copper mesh and stained with uranyl acetate and lead nitrate. Pictures were taken from each section using a transmission electron microscope (Hitachi H-7700, Japan).

Free ferrous iron measurement

Ferrous iron measurement on cells was performed using calcein AM method (Epsztejn et al., 1997). Treated SH-SY5Y cells were incubated with 0.1 M calcein AM (Thermo Fisher Scientific, USA) for 15min. After calcein AM loading, cells were washed and incubated in HBSS. Calcein fluorescence was detected by a SpectraMax i3x Multi-Mode Detection Platform (Molecular Devices, CA, USA) (excitation, 488 nm; emission, 518 nm). Once the signal was stable, iron chelator bipyridyl (200 μM) was added to the well, and the increased fluorescence intensity was recorded.

TMRM and calcein AM staining

SH-SY5Y cells were incubated with 200 nM tetramethylrhodamine methyl ester (TMRM) and 0.1 M calcein AM in HEPES at 37°C for 20 min. Afterwards, cells were washed and observed under a Nikon D-Eclipse C1 confocal

microscope (Nikon, UK).

RPA staining

SH-SY5Y cells were loaded with benzyl ester (RPA) (0.2 μM) in HBSS buffer for 20 min at 37°C, followed by an additional 30 min of incubation in dye-free buffer. Then cells were observed under confocal microscope, or fluorescence was measured using a fluorescence spectrophotometer at 530 nm (excitation) and 590 nm (emission).

Rh-123 staining

SH-SY5Y cells were incubated with 1 μM rhodamine 123 (Rh-123) at 37°C for 20 min. Afterwards, cells were washed and observed under a Nikon D-Eclipse C1 confocal microscope (Nikon, UK).

Quantification and statistical analysis

Two group comparisons were performed by two-tailed Student's t test. Group comparisons (more than two groups) were analyzed using one-way ANOVA followed by Tukey/Kramer's post-hoc test. For some paired experiments (more than two groups), paired two-way ANOVA were applied followed by Tukey/Kramer's post-hoc test. Data is expressed as mean ± SEM. Results were regarded significant at $P < 0.05$.

Supplemental References

BASHKATOVA, V., ALAM, M., VANIN, A. & SCHMIDT, W. J. 2004. Chronic administration of rotenone increases levels of nitric oxide and lipid peroxidation products in rat brain. *Experimental Neurology,* 186**,** 235-241.

DU, F., QIAN, Z., LUO, Q., YUNG, W. & KE, Y. 2015. Hepcidin Suppresses Brain Iron Accumulation by Downregulating Iron Transport Proteins in Iron-Overloaded Rats. *Mol. Neurobiol.,* 52**,** 101-14.

EPSZTEJN, S., KAKHLON, O., GLICKSTEIN, H., BREUER, W. & CABANTCHIK, I. 1997. Fluorescence analysis of the labile iron pool of mammalian cells. *Anal Biochem,* 248**,** 31-40.

ESTORNELL, E., FATO, R., PALLOTTI, F. & LENAZ, G. 1993. Assay conditions for the mitochondrial NADH:coenzyme Q oxidoreductase. *FEBS Lett,* 332**,** 127-31.

HUANG, J., LIU, H., GU, W., YAN, Z., XU, Z., YANG, Y., ZHU, X. & LI, Y. 2006. A delivery strategy for rotenone microspheres in an animal model of Parkinson's disease. *Biomaterials,* 27**,** 937-46.

LI, Q., KO, H., QIAN, Z.-M., YAN, L. Y. C., CHAN, D. C. W., ARBUTHNOTT, G., KE, Y. & YUNG, W.-H. 2017. Refinement of learned skilled movement representation in motor cortex deep output layer. *Nature Communications,* 8**,** 15834.

MEGURO, R., ASANO, Y., ODAGIRI, S., LI, C., IWATSUKI, H. & SHOUMURA, K. 2007. Nonheme-iron histochemistry for light and electron microscopy: a historical, theoretical and technical review. *Arch Histol Cytol,* 70**,** 1-19.

METZ, G. A. & WHISHAW, I. Q. 2009. The ladder rung walking task: a scoring system and its practical application. *J Vis Exp*.

OLSSON, M., NIKKHAH, G., BENTLAGE, C. & BJORKLUND, A. 1995. Forelimb akinesia in the rat Parkinson model: differential effects of dopamine agonists and nigral transplants as assessed by a new stepping test. *J Neurosci,* 15**,** 3863-75.

PERLS, M. 1867. Nachweis von Eisenoxyd in gewissen Pigmenten. *Archiv für pathologische Anatomie und Physiologie und für klinische Medicin,* 39**,** 42-48.

RUMPEL, R., HOHMANN, M., KLEIN, A., WESEMANN, M., BAUMGäRTNER, W., RATZKA, A. & GROTHE, C. 2015. Transplantation of fetal ventral mesencephalic progenitor cells overexpressing high molecular weight fibroblast growth factor 2 isoforms in 6-hydroxydopamine lesioned rats. *Neuroscience,* 286**,** 293-307.

SIMS, N. & ANDERSON, M. 2008. Isolation of mitochondria from rat brain using Percoll density gradient centrifugation. *Nat Protoc,* 3**,** 1228-39.

XU, L. H., XIE, H., SHI, Z. H., DU, L. D., WING, Y. K., LI, A. M., KE, Y. & YUNG, W. H. 2015. Critical Role of Endoplasmic Reticulum Stress in Chronic Intermittent Hypoxia-Induced Deficits in Synaptic Plasticity and Long-Term Memory. *Antioxid Redox Signal,* 23**,** 695-710.